A new view on the trend of solar radiation in mainland China - Based on the optimized empirical model

Zihao Feng
Shandong University of Science and Technology
Bin Guo (guobin07@mails.ucas.ac.cn)
Shandong University of Science and Technology https://orcid.org/0000-0001-7886-0172
Han Xu
Shandong University of Science and Technology
Liguo Zhang
Shandong Provincial Institute of Land Surveying and Mapping
Jie Xu
Shandong Provincial Institute of Land Surveying and Mapping
Ying Xu
Shandong University of Science and Technology

Research Article

Keywords: solar radiation, sunshine duration, empirical model, estimation, trends difference

Posted Date: March 30th, 2021

DOI: https://doi.org/10.21203/rs.3.rs-306411/v1

A new view on the trend of solar radiation in mainland China - Based on the optimized empirical model

Zihao Feng [1,2], Bin Guo [1,2,*], Han Xu [1,2], Liguo Zhang [3], Jie Xu [3], Ying Xu [1,2]

[1] Key Laboratory of Geomatics and Digital Technology of Shandong Province, Shandong University of Science and Technology, Qingdao 266590, China;

[2] College of Geodesy and Geomatics, Shandong University of Science and Technology, Qingdao 266590, China;

[3] Shandong Provincial Institute of Land Surveying and Mapping, Jinan 250102, China

* Correspondence: Bin Guo guobin07@mails.ucas.ac.cn

Abstract: As a kind of renewable energy, the development and utilization of solar energy is valued by many countries. To accurately provide a basis for the use of solar energy in mainland China, the optimized empirical model is adopted to analyze the variation trends and spatial patterns in solar radiation (SR) during 1961-2016 based on the data of 31 SR sites and 500 sunshine duration (SD) stations. The results indicate that there are obvious discrepancies in the variation trends of annual SR and SD during 1961-2016, with trend conversion occurring in 1992 (SR) and 1980 (SD), respectively. Overall, annual SR decreases at the rate of -3.68 MJ/m²·a in China. Notably, SR declines at the rate of -16.95 MJ/m²·a during 1961-1989 ("dimming" stage), while it increases at the rate of 5.34 MJ/m²·a for 1990-2016 ("brightening" period). In addition, all seasons show a tendency of dimming first and then brightening except for autumn. Compared with SD, SR is more sensitive to changes in pollution, leading to a marked recovery with the reduction of pollution after the 1990s. This study provides a new perspective for the trend difference between SR and SD after the 1990s.

Keywords: solar radiation; sunshine duration; empirical model; estimation; trends difference

1. Introduction

The solar radiation reaching the surface of the earth is the main energy source of the planet, provides energy for the movement of the earth's atmosphere, and is also the main source of the earth's light and heat energy (Wild, 2009). Recently, in order to maintain a sustainable development strategy, all energy industries are developing towards low-carbon applications (Pazikadin et al., 2020). Photovoltaic (PV), as a clean energy source, can effectively reduce the consumption of the ozone layer by traditional energy applications and also slow down global warming (Wilberforce et al., 2019). PV generating technology has always been a concern in China. Due to the abundant solar energy, especially in the Northwest region, the application of photovoltaic technology can effectively alleviate the carbon emissions caused by fossil fuels (Gao et al., 2020; Hou et al., 2016). SR is a key factor that determines electricity produced by photovoltaic (PV) systems (Rabaia et al., 2020). Chinese mainland has a vast area, with quite different distribution of SR. Proving the distribution and changes of solar energy in China is a necessary foundation for the stable development of the PV industry (Kazaz and Adiguzel Istil, 2019).

Since the 1950s, the surface solar radiation has been on a downward trend, and this trend continued until the 1980s (global dimming) (Stanhill, 2005). Recent studies have shown that this "dimming" phenomenon ceased in the 1990s (Pinker et al., 2005; Wild, 2005). Additionally, quantities of studies have shown that this dimming stagnation has not continued, but has turned into an upward trend (Augustine and Dutton, 2013; Wild, 2005). The phenomenon where SR decreases first and then increases is widespread all over the world (Augustine and Dutton, 2013; Wild, 2005), and there is a similar trend in China (Che et al., 2005; Wang and Wild, 2016). Since the 1950s, SR has been decreasing in most parts of China (Wang and Wild, 2016), among which, the eastern and central regions have a faster rate of decline, while a few sites in western China show an upward trend (Che et al., 2005; Tao et al., 2016). This is because marginal brightening after 1990 fails to adequately compensate

for strong dimming in the 1950s-1980s (Wang and Yang, 2014). During the dimming phase, SR shows a downward trend in almost all regions of China (Wang and Wild, 2016); on the contrary, in the brightening period, only the western and northeastern regions of China showed a larger upward trend (Tao et al., 2016).

However, SR stations are scarce due to high costs of installation and difficulty in maintenance of measuring instruments (Akinoğlu and Ecevit, 1990). This has led to certain differences in the conclusions drawn by researchers when analyzing SR trends, especially seasonal trends (Wang and Yang, 2014). Insufficient data length and poor site coverage have become the difficult problems in analysis of SR changes in mainland China. In order to overcome the limitations of small data volume and low coverage when analyzing solar radiation changes, the method of using other meteorological elements for auxiliary analysis has gradually been recognized (Zhang et al., 2017). SD is defined as the amount of time when the solar disk is above the horizon and is not obscured by natural obstacles (such as clouds and fog), which is one of the oldest types of radiation measurements (Kaiser and Qian, 2002). SD is considered a high-quality indicator to measure SR (Kaiser and Qian, 2002).

In 1924, *Angström* (Angstrom, 1924) first used the climatological relationship between SD and SR to establish an empirical model. After *Prescott*'s optimization, the model calculation was based on total radiation instead of clear sky radiation (Prescott, 1940). Since then, various variants of the *Angström* model have evolved, such as logarithmic model (Black et al., 1954), power function model (Coppolino, 1994), and so on. These models have been widely used in the simulation of SR around the world (Fan et al., 2019; Zhang et al., 2017). Subsequently, SR calculation models based on various meteorological elements (cloud cover (Súri et al., 2005), temperature (Hassan et al., 2016) and combined weather model (Zeng et al., 2019)) has also been established and applied. Although these models have better performance in some areas, they also have instability due to higher data requirements (Zhang et al., 2017). Due to the validity and reliability of the SD data measured by most weather

77 stations in the world, the empirical model based on SD is still the most extensively used
78 model for SR estimation (Al-Mostafa et al., 2014).

79 The empirical model is a linear model, and it cannot adjust itself according to changes
80 in element relationships. Due to the instability of SR and SD since the 1950s, their changes
81 are not the same (Wang and Yang, 2014). This different trend change among the two
82 elements is likely to cause errors in the calculation of SR. *Liu et al.* (Liu et al., 2015) find
83 that *Angström* model performs best when calibrated with a 10-year data set. We can
84 cautiously assume that the different relationship between SR and SD affects the calculation
85 accuracy of the empirical model. However, there is no optimization of the empirical model
86 based on the different trends of the two elements.

87 Therefore, the objectives of this present study are to: (1) address the similarities and
88 differences between SR and SD from 1961 to 2016, and optimize the selected empirical
89 model based on these results; (2) calculate the SR of mainland China, and analyze the
90 temporal and spatial change trends; and (3) explore the possible reasons for similarities and
91 differences in SR and SD.

92 **2. Materials and Methods**

93 2.1. Study Area

94 This study is conducted over mainland China, located within 73°41′-135°02′E and
95 18°10′-53°33′N. The geography of mainland China is variable and the topography has
96 obvious regional differences. There are many climate types in mainland China, covering
97 monsoon climate, continental climate and plateau climate from east to west. The climatic
98 conditions of each climatic zone are obviously different. Therefore, based on indicators such
99 as heat and precipitation, combined with China's main climate types, mainland China is
100 divided into 8 climate regions (Table 1). Fig. 1 shows the geographical details of each
101 partition.

102 **Table 1** Climate regions of mainland China in this study.

Climate Region		Climate Type
Northeastern China	(NE)	Cold temperate monsoon climate, monsoon climate of medium latitudes
Inner Mongolia Area	(IM)	Monsoon climate of medium latitudes, cold temperate monsoon climate
Gan-Xin Area	(GX)	Cold temperate, temperate, warm temperate climate
North China	(NC)	Warm temperate monsoon climate
Central of China	(CC)	Subtropical monsoon climate
Southern China	(SC)	Subtropical, tropical monsoon climate, equatorial monsoon climate
Chuan-Dian Area	(CD)	Plateau monsoon climate
Qinghai-Tibet Area	(QT)	Plateau climate

103 2.2 Data

104 Daily SR data from 130 stations and SD data from 753 stations during January 1961 to
105 December 2016 have been provided by the National Meteorological Information Center of
106 the China Meteorological Administration (http://data.cma.cn). All observations provided by
107 these stations are subject to strict quality control. The stations with continuous data and time
108 series length of 56 years or more are selected, and those sites are deleted with continuous
109 missing measurement for more than two months or total missing measurement for more than
110 missing measurement for more than two months or total missing measurement for more than
111 six months. After screening, 31 SR and 500 SD stations are retained (Fig. 1). SR sites are
112 evenly distributed except QT region, and SD sites have a similar distribution pattern, but the
113 density is higher. The daily air pollution index (API) data of 120 cities in mainland China
114 from March 2001 to December 2012 are obtained from China Environmental Monitoring
115 Center (http://www.cnemc.cn/). In this study, seasons are defined as winter (December-
116 February), spring (March-May), summer (June-August), and autumn (September-November).

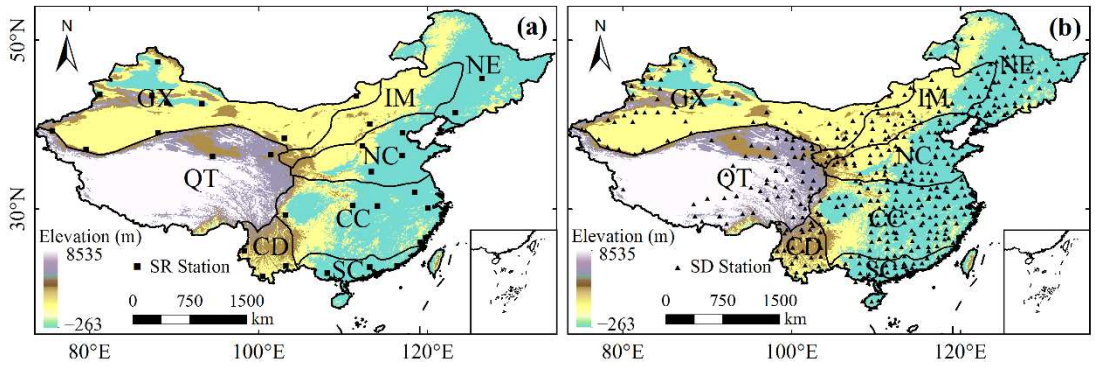

Fig. 1 Digital Elevation Model (DEM), eight climate regions and locations of (a) SR; and (b) SD stations in mainland China.

2.3. Methods

2.3.1 Time series analysis method

In this study, the temporal trend is analyzed by using linear trend analysis, mutation test, and significance test, and Universal Kriging spatial interpolation method was used to analyze spatial changes (Hu et al., 2003; Ren et al., 2017). Mann-Kendall (M-K) nonparametric test can be very effective for testing time series (Kendall, 1948). In this study, the changing trend and tendency significance of SR in mainland China are presented by using M-K test. The Mann-Kendall rank statistics is a common method for testing abrupt change in time series (Sang et al., 2014). In this method, the mutation time is usually determined by the intersection of the UF and UB curves. However, this single mutation time determination method is susceptible to disturbances such as the length of the time series and the step size. Therefore, this study combines Bernaola-Galvan (B-G) segmentation algorithm (Bernaola-Galván et al., 2000), Move-t, Ymamoto and Lepage test methods to determine the mutation time of SD in mainland China. Among them, B-G test is an excellent visual mutation test method, which can divide the interval according to the mutation time (Feng et al., 2005).

135 2.3.2 Solar radiation simulation method

136 Six empirical models are used in this study, combined with the measured values of SR
137 in mainland China to verify the applicability of the model. Firstly, the extraterrestrial
138 radiation (S_0) and possible daily SD (H_0) are calculated.

139 $$S_0 = \frac{24 \times 3600}{\pi} G_{sc} k \left(\cos\phi \cos\delta \sin\omega_s + \frac{\pi \omega_s}{180} \sin\phi \sin\delta \right) \quad (1)$$

140 where G_{sc} is the solar constant (=1367 W/m^2 (Duffie et al., 1991)); and k is the eccentricity
141 correction coefficient:

142 $$k = 1 + 0.033 \left(\cos\frac{360n}{365} \right) \quad (2)$$

143 where n is the day of the year starting on 1 January. The magnetic declination δ and the sunset
144 angle ω_s can be calculated according to Cooper's equation (Cooper, 1969):

145 $$\delta = 23.45 \sin\left(360 \frac{284 + n}{365} \right) \quad (3)$$

146 $$\omega_s = \cos^{-1}\left(-\tan\phi \tan\delta \right) \quad (4)$$

147 where φ is the local latitude. The possible daily SD (H_0) can be calculated by the following
148 formula (Iqbal, 1983):

149 $$H_0 = \frac{2\omega_s}{15} \quad (5)$$

150 According to Formulas 1-5, the extraterrestrial radiation (S_0) and possible daily SD (H_0)
151 can be used to simulate SR. Considering the applicability of the model, six kinds of daily
152 empirical models are selected for various climatic types (Table 2).

153 The performance of the models is evaluated on the basis of the following statistical error
154 tests. Coefficient of determination (R^2):

$$R^2 = \frac{\sum(\hat{y} - \bar{y})^2}{\sum(y - \bar{y})^2} \quad (6)$$

Mean absolute bias error (MABE):

$$MABE = \frac{1}{n}\sum_{i=1}^{n}\left|R_M - R_S\right| \quad (7)$$

where R_M and R_S represent simulation and measured values respectively; and n is the total number of observations

Root mean square error (RMSE):

$$RMSE = \sqrt{\frac{1}{n}\sum_{i=1}^{n}\left(R_M - R_S\right)^2} \quad (8)$$

Table 2 Empirical models proposed in literature.

Models	Mod. no.	Empirical equation	Source
Linear	a	$\frac{S}{S_0} = a + b\frac{H}{H_0}$	Prescott (Prescott, 1940)
Quadratic	b	$\frac{S}{S_0} = a + b\frac{H}{H_0} + c\left(\frac{H}{H_0}\right)^2$	Akinoglu (Akinoğlu and Ecevit, 1990)
Cubic	c	$\frac{S}{S_0} = a + b\frac{H}{H_0} + c\left(\frac{H}{H_0}\right)^2 + d\left(\frac{H}{H_0}\right)^3$	Bahel (Bahel et al., 1987)
Modified logarithmic	d	$\frac{S}{S_0} = a + b\log\left(\frac{H}{H_0} + 1\right)$	Fan (Fan et al., 2019)
Linear logarithmic	e	$\frac{S}{S_0} = a + b\frac{H}{H_0} + c\log\left(\frac{H}{H_0} + 1\right)$	Fan (Fan et al., 2019)
Exponential	f	$\frac{S}{S_0} = a + b\exp\left(\frac{H}{H_0}\right)$	Almorox (Almorox and Hontoria, 2004)

3. Results

3.1 Comparison of variation characteristics of SR and SD

In order to optimize the empirical model of SR, the variation trends of SR and SD are compared in mainland China from 1961 to 2016 (Fig. 2). Both SR and SD show a downward trend after 1961. The decline trend of SR stops around 1990, and then there is an obvious

rebound tendency. *Wang et al.* (Wang et al., 2013) and *Wild et al.* (Wild et al., 2009) reached a similar conclusion. However, SD shows a decreasing trend from 1961 to 2016, and an abrupt drop in the early 1980s. This tendency is also have been drawn by *Chen et al.* (Chen et al., 2010). Four mutation detection methods are used to detect the mutation of two meteorological elements. The main mutation time of SR occurs in 1992 and that of SD occurs in 1980 (Table 3).

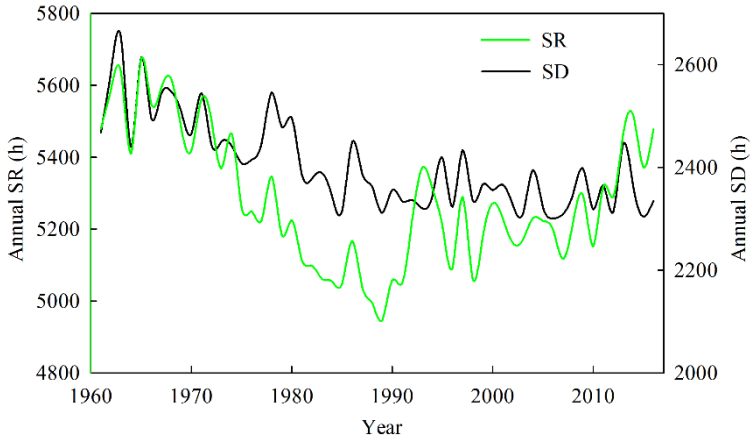

Fig. 2 Comparison of the annual mean values of SR and SD in 31 sites during 1961-2016.

Table 3 Signal of abrupt change in SR and SD in mainland China during 1961-2016.

	Mann-Kendall	Yamamoto	Move-*t*	LePage
SR	1969	1992	1992	1992
SD	1980	1980	1980	1980

SR and SD show a decreasing trend in mainland China during 1961-2016 (Table 4), with tendency rates of -4.485 MJ/m²·a and -4.018 h/a, respectively. There are significant differences in trend rate between SR and SD in different time periods (divided by the mutation time). During 1961-1979, the decrease rate of SR is the largest in all time periods (-20.468 MJ/m²·a), while SD also shows a large downward trend (-6.170 h/a). In the 1980s, SD has a sudden decline tendency, and the downward trend increases (-8.344 h/a), while the decline trend of SR in the same period slightly slows down (-13.145 MJ/m²·a). After that, SR shows an obvious rising trend (7.544 MJ/m²·a). In the same period, the decrease trend of SD

185 slows down and tends to be stable (-0.418 h/a).

186 **Table 4** Difference between SR and SD before and after mutation.

Time	SR Trend (MJ/m²·a)	SD Trend (h/a)
1961-2016	-4.485	-4.017
1961-1979	-20.468	-6.170
1980-1991	-13.145	-8.344
1992-2016	7.554	-0.418

187 3.2 Model optimization and simulation of SR

188 In order to ensure the reliability of the simulation results, the consistency of six
189 empirical models is evaluated. The measured values of 31 high-quality SR stations are
190 selected as the real values. Firstly, the coefficients of the six empirical models are determined
191 by the relationship between the measured SR/extraterrestrial radiation (S/S_0) and the
192 measured SD/theoretical SD (H/H_0). According to the coefficient determined by regression
193 relation, coefficient and R^2 of empirical models are obtained (Table 5).

194 The correlation between the predicted values and measured values of the six empirical
195 models is analyzed (Fig. 3). It can be seen that all the six models can well estimate SR value,
196 but with certain differences in fitting degree and error quantity. Among the six models, Cubic
197 model shows the best correlation. In addition, Cubic model has the minimum error value,
198 followed by the Quadratic and Linear logarithmic model. This indicates that Cubic model
199 has the best goodness of fit. Similar conclusion has been drawn by *Zhang et al.* (Zhang et al.,
200 2017) and *Yao et al.* (Yao et al., 2018). Therefore, Cubic model is selected for SR simulation
201 in this study.

202 Obvious mutations in SD and SR occur in 1980 and 1992 respectively during 1961-
203 2016. The trends of SD and SR have obvious discrepancies in different periods separated by
204 two time points. Four coefficients of the Cubic model per year are calculated, and the changes
205 of each coefficient in the study period (including B-G analysis) are given respectively (Fig.
206 4). B-G test shows that four coefficients in the empirical model all had the mean mutation in

1992, and b, c, d have an obvious mean mutation in 1980. This indicates that the correlation between SR and SD changes at these two time points. Therefore, combining the trend conversion of SR (1992) and SD (1980) and the mean mutation of empirical model coefficient (1980 and 1992), we conduct segmented simulations on SR to minimize estimation errors.

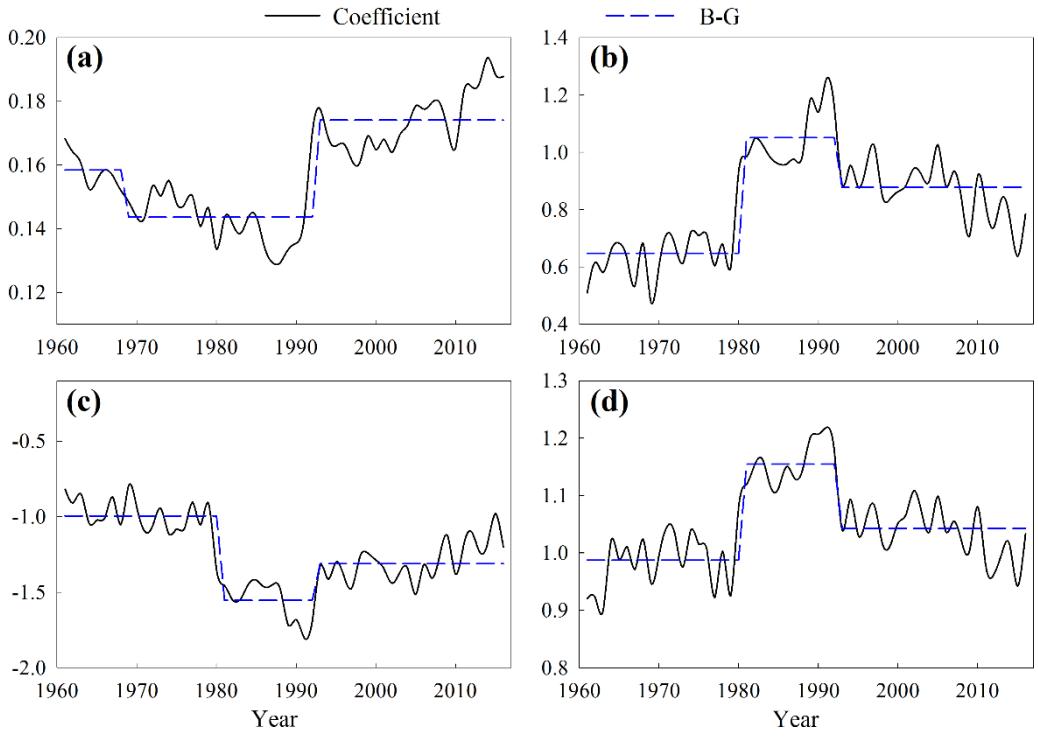

Fig. 4 Changes in four coefficients of the Cubic model, 1961-2016. (a), (b), (c) and (d) represent the a, b, c, d coefficients, respectively (Blue line is different mean segmentation obtained by B-G test, and conversion point is mutation time).

Fig. 5 shows the comparison of the agreement between predicted and measured values in different time periods before and after model optimization. The optimized model shows better coherence in all the three time periods. During 1980-1991, the consistency significantly improves after model optimization, with RMSE significantly reduced and R^2 increased. From 1992 to 2016, the tendency of SR changes from declining to increasing, and SD changes from a significant downward trend to a stable fluctuation trend. During this period, RMSE of the

optimized model is also significantly lower than that of pre-optimized model. Overall, R^2 of the optimized model increases; MABE decreases, and RMSE significantly reduces.

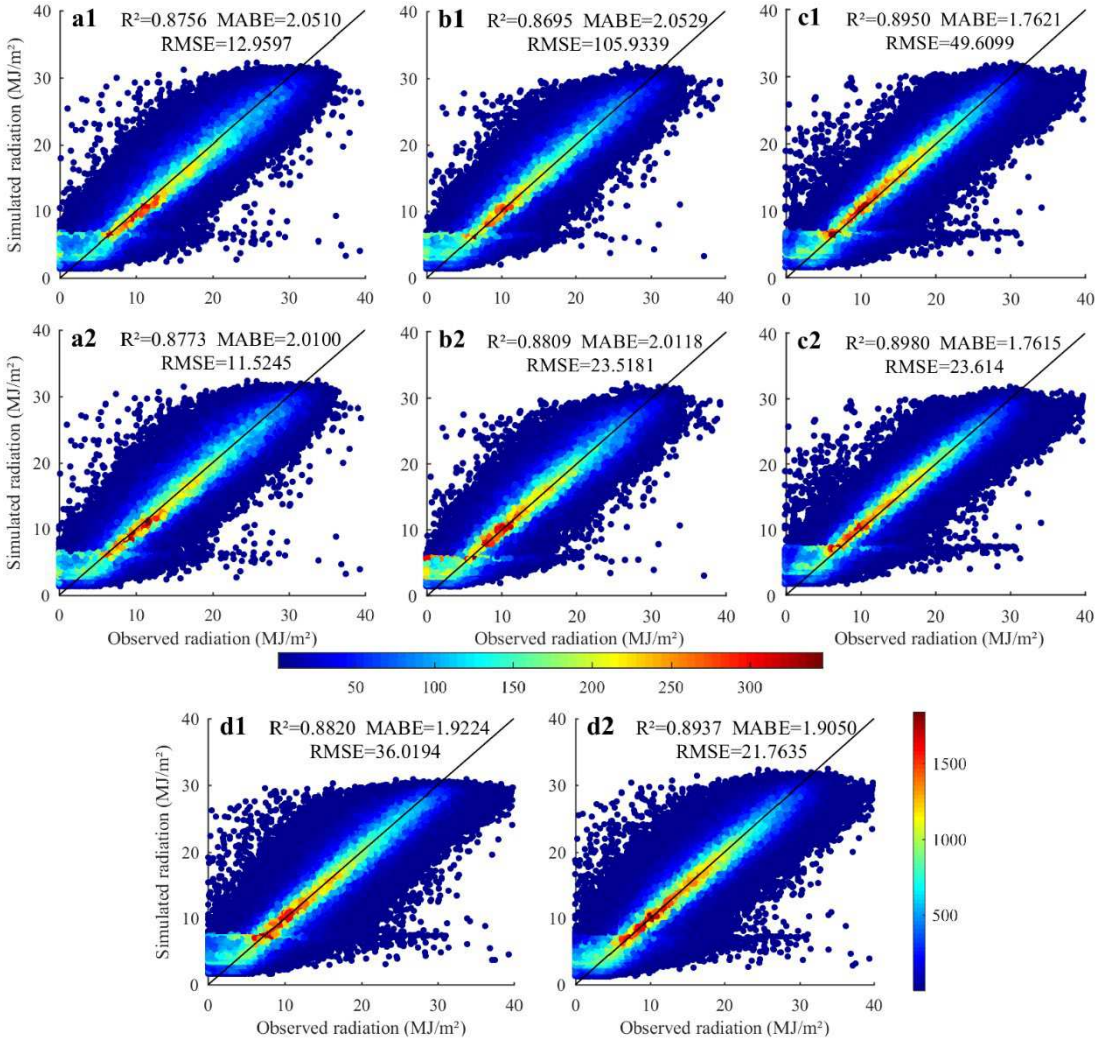

Fig. 5 Comparison of simulated and measured values before and after model optimization in different periods (a, b, c and d represent the period of 1961-1979,1980-1991,1992-2016 and 1961-2016 respectively; 1 represents the pre-optimized model and 2 is the post-optimized model. Time period segmentation by primary mutation time of SR. The color of the dots indicates the density of the dots; the red dots are the area with higher density; black line is $y=x$).

In order to further analyze the estimation effect of the model before and after optimization, the annual average daily SR calculated by the models is compared with the

measured value (Fig. 6a). The optimized model is obviously closer to the measured value. And the optimized model performs better in showing the rapid decline in SR from the late 1970s to the early 1990s. After the 1990s, both models show an upward trend of SR, but the difference between the optimized model and the measured value is smaller (Fig. 6b). To sum up, the optimized model has higher consistency with the observed value and therefore can better reflect the dimming and brightening trend of SR.

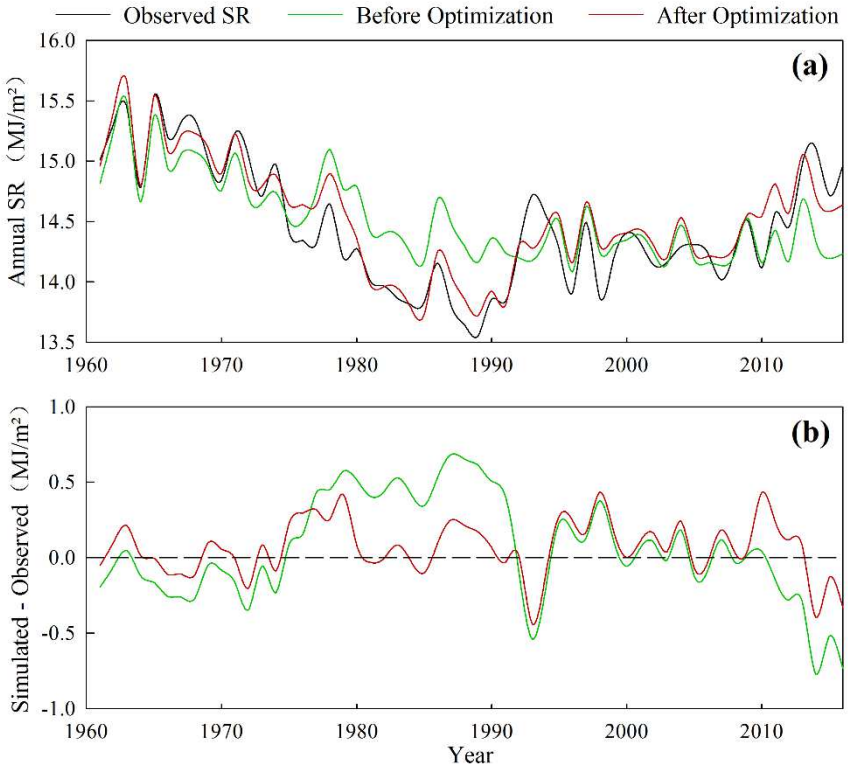

Fig. 6 Comparison between simulated and measured values of models before and after optimization: (a) daily radiation exposures; (b) simulated values minus measured values.

3.3 Temporal and spatial variations of SR based on simulated values

3.3.1 Spatial variation of SR

Fig. 7 shows the spatial distribution of annual average SR and tendency rate over mainland China during 1961-2016 (based on simulated data). The annual average SR in mainland China is more in the southeast and less in the northwest (Fig. 7a). In eight climate

regions, GX and QT regions have the highest average annual SR (7000 MJ/m²), which is due to the high altitudes of the two regions and climatic reasons that lead to scarce precipitation. In contrast, the area with the shortest annual average SR is located in the west of CC, and its minimum value is less than 3500 MJ/m². This is due to the basin topography and circulation factors accumulated a large number of clouds, fog (Lu and Ye, 2011). Frequent precipitation is the main factor for low SR in CC.

Over the period 1961-2016, the annual average SR in most of the mainland China showed a downward trend (Fig. 7b). Among them, NC and CC have the largest decline in SR, especially in central NC and southern CC (trend rate exceeds -12MJ/ m²·a). The largest drop in SR in these two regions is related to the pollution brought by the rapid development of economy (Wang et al., 2014). On the contrary, there is an increasing trend in the west of QT and CD, and there are also some areas in the middle and west of GX that show the same trend.

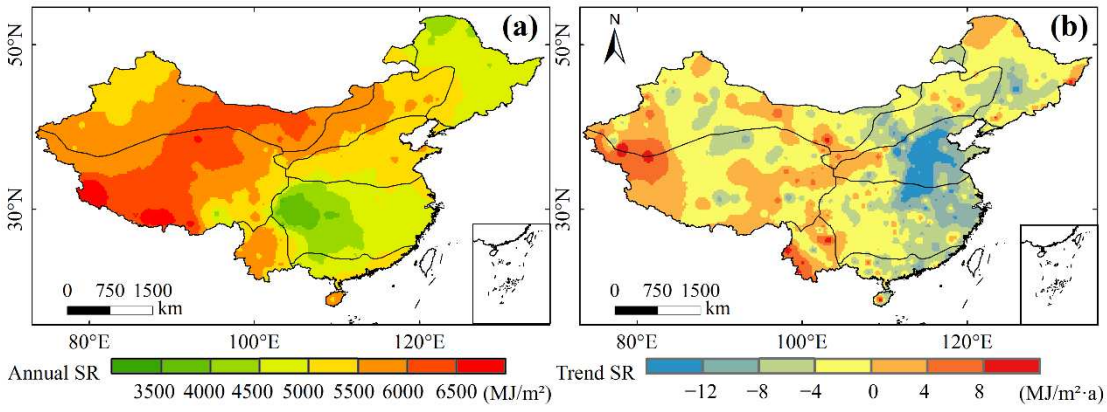

Fig. 7 Spatial distribution of (a) annual SR; and (b) tendency rate in mainland China during 1961-2016.

Since SR seasonal distribution is similar to annual distribution with only a difference in magnitude, this study only analyzes the seasonal variation trend of SR (Fig. 8). In general, the rising trend of SR is the most obvious in spring, while the decreasing trend is the largest in summer. And the SR decline rate in all seasons in the eastern region is higher than that in

the western region. The northwest of QT region shows the largest upward trend in spring, while the area with more concentrated downward trend is NC. Besides, the tendency of SR is similar in summer, autumn and winter, and NC is the region with the largest decline, followed by CC. QT and CD show the largest upward trend.

3.3.2 Trends of SR in mainland China

Fig. 9a shows a suspected trend mutation of SR in mainland China in the late 1980s. MK test is used to test the change in SR trend (Fig. 9b), and the tendency of annual SR changes significantly around 1989. This result is the same with that obtained by *Wang et al.* (Wang and Wild, 2016). According to the time of the trend transformation, SR is divided into 1961-1989 dimming stage and 1990-2016 brightening stage in mainland China. The annual SR in mainland China shows a significant downward trend of -16.95 MJ/m²·a in 1961-1989 (p<0.01), reaching a minimum value of 4901.11 MJ/m² in 1989. Among them, the largest decline appears in the 1980s, 5.43% lower than that in the 1970s. From 1990 to 2016, the SR increases by 5.34 MJ/m²·a (p<0.05) in mainland China, with the largest increase in the 1990s, an increase of 2.67% over the 1980s.

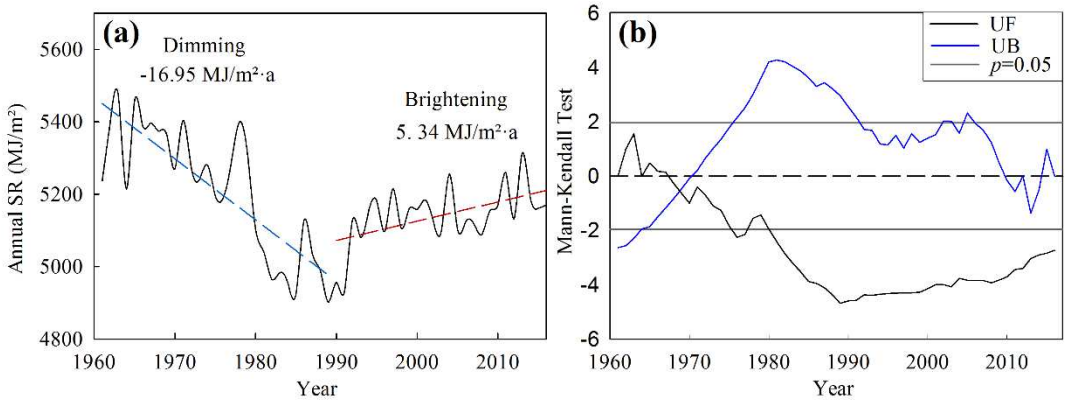

Fig. 9 (a) Trends in annual SR; (b) Mann-Kendall test results based on simulated values during 1961-2016 in mainland China.

The seasonal trend of SR in Mainland China is analyzed (Fig. 10). In the dimming phase of 1961-1989, SR of each season has a significant downward trend, all passing the p<0.05

significance test. Among them, the maximum decline rate of SR is in summer (-6.22 MJ/m²·a), followed by spring, autumn and winter, with trend rates of -4.55, -3.04 and -2.99 MJ/m²·a, respectively. During the brightening period from 1990 to 2016, the season with the most significant SR upward trend is spring (3.76 MJ/m²·a), followed by winter (1.34 MJ/m²·a). On the contrary, the upward trend in summer is not significant, and SR in autumn still shows a downward trend after a slight rebound in the early 1990s. Similar conclusion has been drawn by *Wang et al.* (Wang and Wild, 2016).

Table 6 analyzes the variation trend of SR in eight climatic regions in 1961-2016 based on simulated values. From 1961 to 2016, SR shows a downward trend in most regions of mainland China. Among them, SR decline trend rate in NC is the largest (-8.22 MJ/m²·a), followed by CC and SC, with trend rates of -5.67 and -4.74 MJ/m²·a, respectively. CD is the only region with an upward trend (2.46 MJ/m²·a). Due to the instability of SR (dimming and brightening), only half of the regions have passed the $p<0.05$ significance test. Except for NC region, SR of all regions shows a trend of decreasing first and then increasing. Therefore, the phenomenon of dimming and brightening is very common in mainland China. From 1961 to 1989, SR has a significant downward trend in each subregion. Among them, CC, SC and NC regions have the largest decline rates, -26.20, -24.38 and -20.13 MJ/m²·a, respectively. In the brightening period, SR of the seven sub-regions all rebounds to a certain extent with the exception of North China. Among them, CD region has the largest upward trend rate (20.68 MJ/m²·a), followed by SC and GX, with trend rates of 8.78 and 8.77 MJ/m²·a, respectively. North China is the only region with a downward trend in both periods, which is similar to the conclusion by *Zheng et al.* (Zheng et al., 2012).

4. Discussion

Between 1961 and 2016, both SR and SD show a different downward trend in mainland China. The trend of SR changes in the late 1980s, from decreasing to increasing, consistent

with the findings of *Wang et al.* (Wang et al., 2013). However, after a rapid decline in SD in the 1980s, the trend gradually stabilizes, as is also reported by *Song et al.* (Song et al., 2019) and *Feng et al.* (Feng et al., 2019).

Table 6 Variations of SR in subregions based on simulated values from 1961-2016 (* refers to passing $p<0.05$ significance).

	NE	IM	GX	NC	CC	SC	CD	QT
1961-2016 (MJ/m²·a)	-3.16*	-3.75*	-0.82	-8.22*	-5.67*	-4.74	2.46	-0.23
Dimming (MJ/m²·a)	-12.96*	-11.84*	-11.48*	-20.13*	-26.20*	-24.38*	-11.22*	-5.30*
Brightening (MJ/m²·a)	3.08	4.83*	8.77*	-4.00	4.92	8.78*	20.68*	5.54*

Six empirical models are verified with the measured data of 31 radiation sites as true values, among which the cubic model shows the best consistency. In addition, this study finds the limitations of the linear regression model, and then proposes to optimize the model based on the trend transition points of SR and SD. After optimization, the consistency of the model is obviously improved. Before and after the trend conversion point, the correlation between the two and the regression coefficient are significantly different (Table 3 and Fig. 4).

The obvious variation of correlation is caused by the unsynchronized trends in SR and SD. Based on the optimized model, SR shows an overall downward trend in mainland China from 1961 to 2016, divided into the 1961-1989 dimming stage and the 1990-2016 brightening stage. This trend conversion phenomenon is also pointed out by *Wild et al.* (Wild, 2012). From 1961 to 2016, SR decline rate was the largest in NC, followed by CC and SC. Except for autumn, all seasons show a trend of dimming first and then brightening. The degree of dimming is the greatest in winter and the trend of rebound is the most significant in spring. Similar conclusions have been drawn by *Wang et al.* (Wang and Wild, 2016).

Changes in SR and SD are always related to factors such as aerosol, wind speed and precipitation (Fei and Xia, 2015; Luo et al., 2019). As an indicator closely related to aerosol

optical thickness (AOD), the level of air pollution index (API) has a significant impact on SR and SD (Wang et al., 2014). 58 API sites are selected in mainland China from 2001 to 2012 (Table 7), which are divided into two groups for comparison (based on a median of 75). It can be seen that the annual and seasonal declines in SR and SD are greater in areas with larger API. This also explains that as the most polluted area in mainland China, NC has the most significant decline in SR. Since 1990, Chinese mainland AOD has declined (Wang et al., 2013), as is evidenced by the API trends of 2001-2012. This is one of the important reasons for the rebound of SR and SD. Besides, the trend shift is analyzed of wind speed, precipitation and relative humidity around 1989 (Fig. 11). Among them, the trends of wind speed before and after 1989 are significantly different, and the relative humidity has the same performance. The decline rate of wind speed slows down significantly, and an abrupt change signal is detected in the MK test in 1989. *Lin et al.* (Lin et al., 2015) point out that the reduction of wind speed magnifies the weakening effect of aerosol on SR and SD. The downward trend of wind speed slows down after 1989, and there is a trend of recovery around 2010. Relative humidity is closely related to water vapor which has a certain weakening effect on SR (Yang et al., 2009). The rapid decline of relative humidity has a certain correlation with the trend of SR recovery after 1989.

Table 7 Trends of annual and quarterly SR and SD with average API<75 and≥75.

	Trend of SR (MJ/m²·a)					Trend of SD (h/a)				
	Ann	Spr.	Sum.	Fal.	Win.	Ann	Spr.	Sum.	Fal.	Win.
API<75	-6.45	-0.47	-2.73	-1.49	-1.09	-5.69	-0.70	-2.19	-1.43	-1.37
API≥75	-8.50	-0.49	-4.16	-2.00	-1.85	-7.82	-0.81	-3.03	-1.88	-2.09

In addition to similar trends, there are significant differences in the trends of SR and SD after the 1980s (Fig. 2). Explanation of this phenomenon is attempted from the different response degrees of SR and SD to pollution. Cities with API stations, SD stations, and first-class SR stations are selected as research targets (Fig. 12). The percentage difference in clear

sky conditions is compared between SR and SD under light pollution conditions and under heavy pollution conditions. When the amount of diffuse radiation reaching the earth's surface is less than or equal to 25% of global radiation, the sky is termed as clear sky (Ahmad and Tiwari, 2011). The results indicate that SR and SD of the days with less pollution are greater than that of the days with severe pollution in almost all stations in each season. This shows that air pollution has a certain weakening effect on SR and SD. The heavier the air pollution, the more obvious the weakening effect. Moreover, the difference of SR under the two pollution conditions is greater, which indicates that the response degree of SR to pollution may be more sensitive than SD. From the early 1990s to 2005, various pollution indicators show a downward trend in China's large cities, as reported by *Chan et al.* (Chan and Yao, 2008), and this is consistent with the trend of API change during 2001-2012 (Fig. 11). Combined with the difference in the response degree of SR and SD to pollution, the trend difference between SR and SD after the 1990s may be due to the fact that SR is more sensitive to pollution reduction. The decline in SR (-9.74%) from 1961 to 1989 is significantly greater than SD (-6.34%), which also proves this point of view. A possible reason for the stronger response of SR to pollution is inferred: SD meter only responds to radiation greater than 120 W/m^2 (Xia, 2010). Under clear sky conditions, the weakening effect of pollution on SD only has an effect at sunrise and sunset. In contrast, the response of SR, weakened by pollution throughout the day, is more obvious.

Though the main objectives of the study have been achieved, it must be acknowledged that there are still some uncertainties in the present study. (1) Due to data limitations, it is difficult to obtain pollution data before 2000, which also makes it impossible to quantitatively explain when analyzing the common downward trend of SR and SD. (2) Although the theory proposed in this study can explain the difference between SD and SR changes well, the sudden rise in SR around 1992 is still puzzling. Based on previous studies (Feng et al., 2019), we cautiously conjecture that this sudden change may be related to the dissipation of volcanic

aerosols accumulated in the atmosphere from the 1980s to the early 1990s.

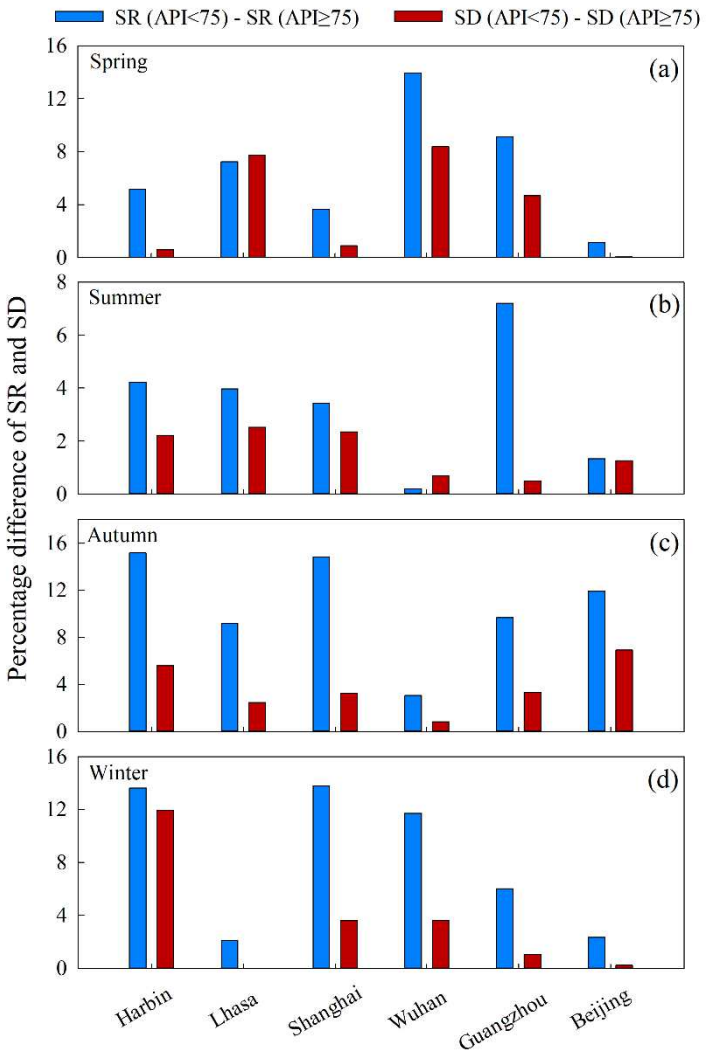

Fig. 12 Responses of SR and SD to different pollution levels under clear sky in (a) spring; (b) summer; (c) autumn; and (d) winter (The blue column indicates the percentage difference between SR when API<75 and API≥75, and the red column indicates the percentage difference between SD when API<75 and API≥75).

5. Conclusion

In this study, the similarities and differences between SR and SD during 1961-2016 are explored, and the Cubic empirical model with the best consistency of six models is selected. The model is optimized according to the trend conversion time of SR and SD. Finally, based on the optimized model, temporal and spatial changes of SR are analyzed in mainland China.

The result shows that SR shows a downward trend in mainland China from 1961 to 2016, divided into the 1961-1989 dimming stage (-16.95 MJ/m²·a) and the 1990-2016 brightening stage (5.34 MJ/m²·a). Except for autumn, all seasons shows a tendency to dimming first and then brightening. The degree of dimming is the greatest in winter and the trend of rebound is the most significant in spring. From 1961 to 2016, the decline rate of SR is the largest in NC, followed by CC and SC. Except in NC, SR shows the trend of dimming and then brightening in mainland China. North China shows a downward trend in both periods, which may be related to worse local pollution. During the brightening period, most areas show an upward trend in spring; however, only western China shows a small upward trend in autumn.

The downward trend of SR and SD from 1961 to 1989 may be due to more serious pollution, while the trend changes after the 1990s is related to the stagnation of the downward trend of wind speed, pollution mitigation and the rapid decline of relative humidity. The trend difference between SR and SD after the 1990s may result from the fact that SR is more sensitive to pollution reduction.

Declarations

Funding

This work is funded by the National Natural Science Foundation of China (41807170), the Major Science and Technology Innovation Projects of Shandong Province (2019JZZY020103), the Talent Introduction Plan for Youth Innovation Team in Universities of Shandong Province (Innovation Team of Satellite Positioning and Navigation) and the Opening Fund of Key Laboratory of Geomatics and Digital Technology of Shandong Province.

Competing interests

The authors declare that they have no known competing financial interests or personal

relationships that could have appeared to influence the work reported in this paper.

Availability of data and material

The datasets analyzed during the current study are available in the National Meteorological Information Center of the China Meteorological Administration (http://data.cma.cn) and China Environmental Monitoring Center (http://www.cnemc.cn/).

Authors' contributions

Zihao Feng: Data curation, Writing- Original draft preparation. **Guo Bin**: Supervision, Writing- Reviewing and Editing. **Han Xu**: Visualization, Investigation. **Liguo Zhang**: Data handling. **Jie Xu**: Data analysis. **Ying Xu**: Methodology.

Ethics approval

The results of this study are clear and honest, without fabricating, falsification or improper data manipulation (including image-based manipulation). Authors have adhered to discipline-specific rules for acquiring, selecting and processing data. No data, text, or theories by others are presented. This manuscript has not submitted to more than one journal for simultaneous consideration. This submitted work is original and will not be published elsewhere in any form or language.

Consent to participate

Not applicable.

Consent for publication

Not applicable.

Appendices

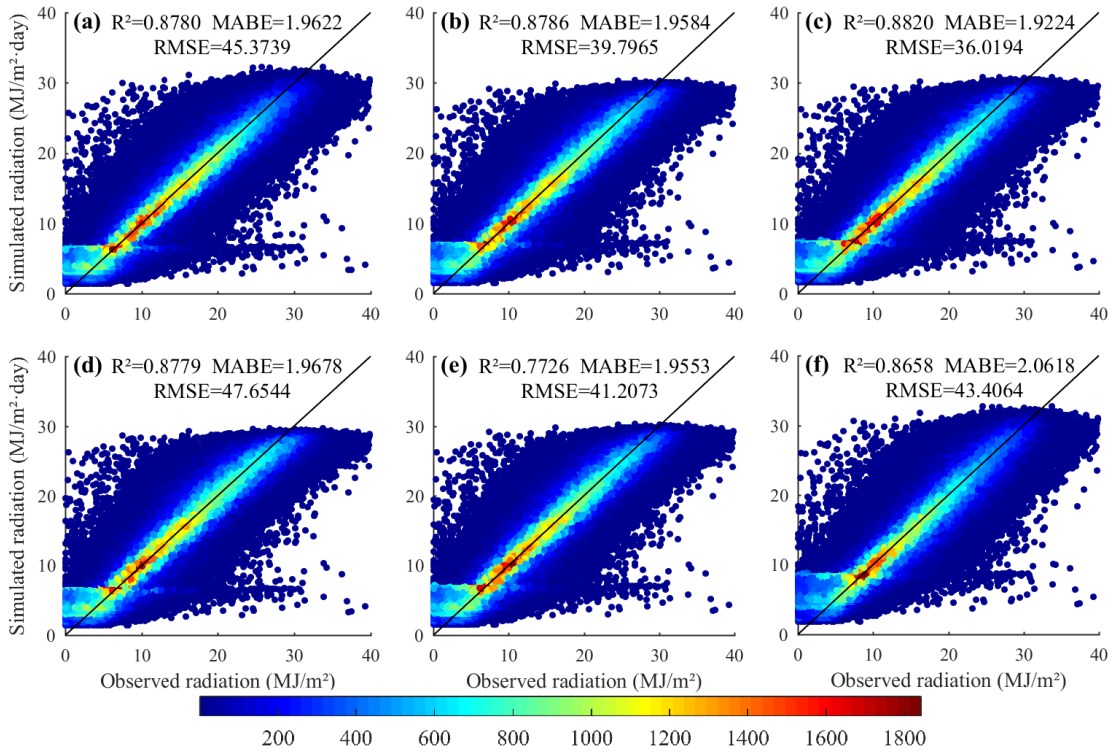

Fig. 3 Comparison and error analysis of six models (a) Liner model; (b) Quadratic model; (c) Cubic model; (d) Modified logarithmic model; (e) Linear logarithmic model; and (f) Exponential model (The color of the dots indicates the density of the dots; the red dots are the area with higher density; and black line is $y=x$).

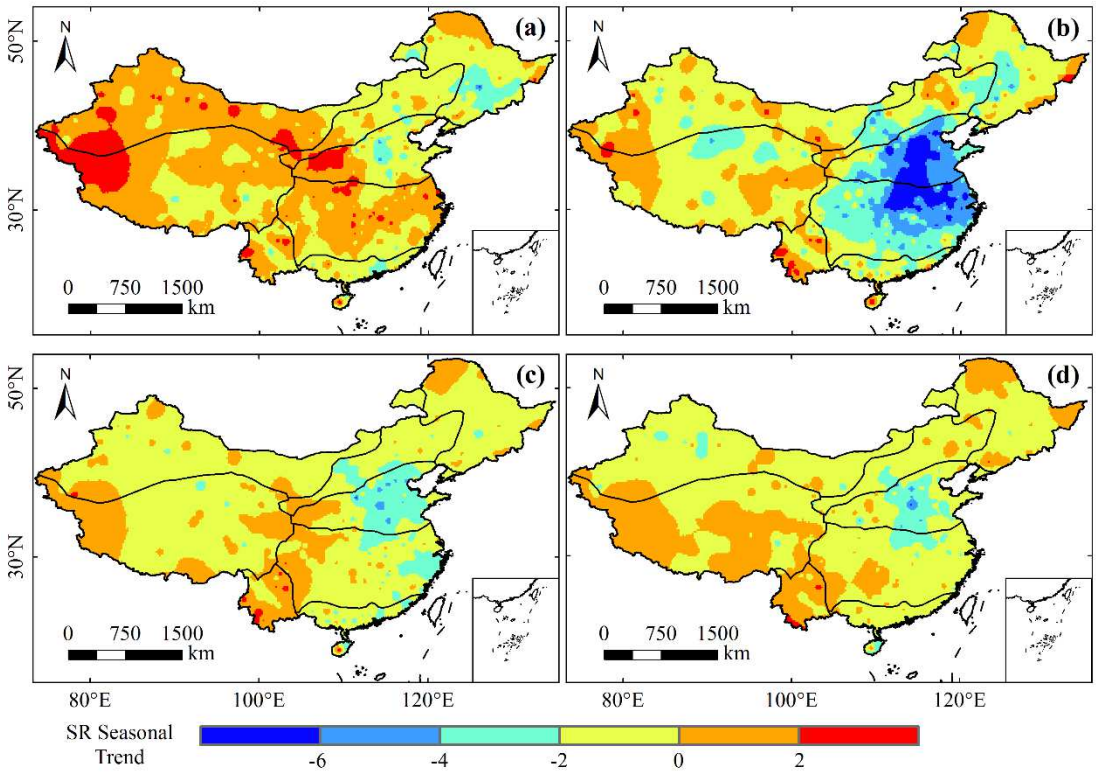

Fig. 8 Spatial distribution of seasonal SR in mainland China during 1961-2016 for (a) spring; (b) summer; (c) autumn; and (d) winter.

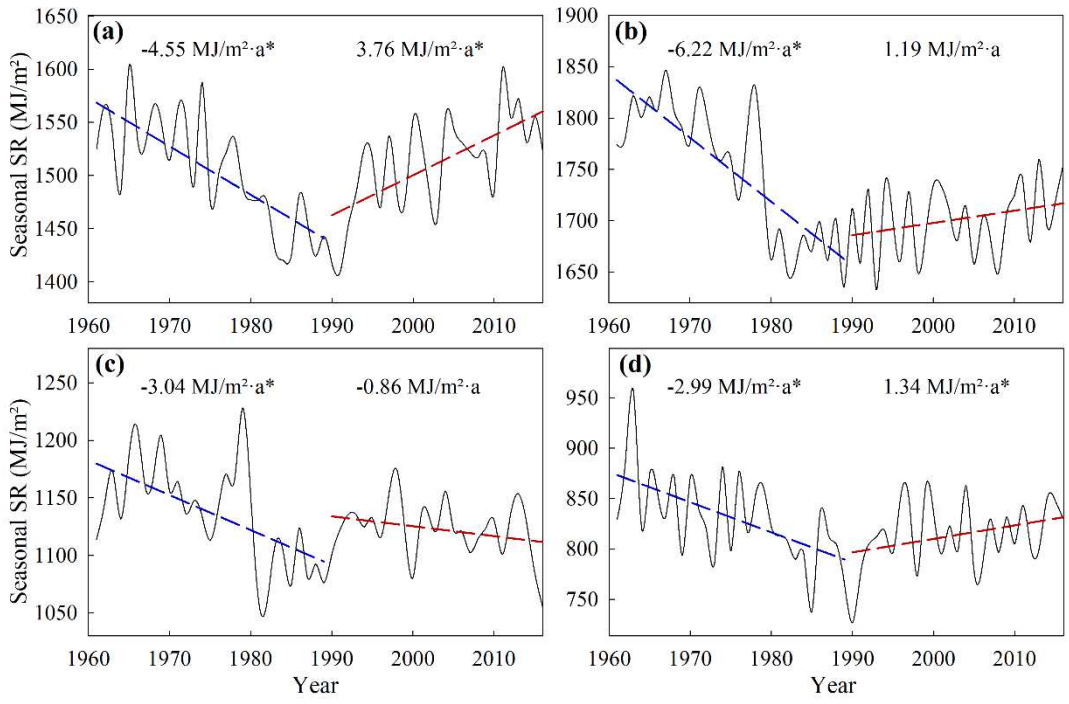

Fig. 10 Variations of SR based on simulated values for (a) spring; (b) summer; (c) autumn; and (d) winter in mainland China during 1961-2016 (* refers to passing p<0.05 significance test).

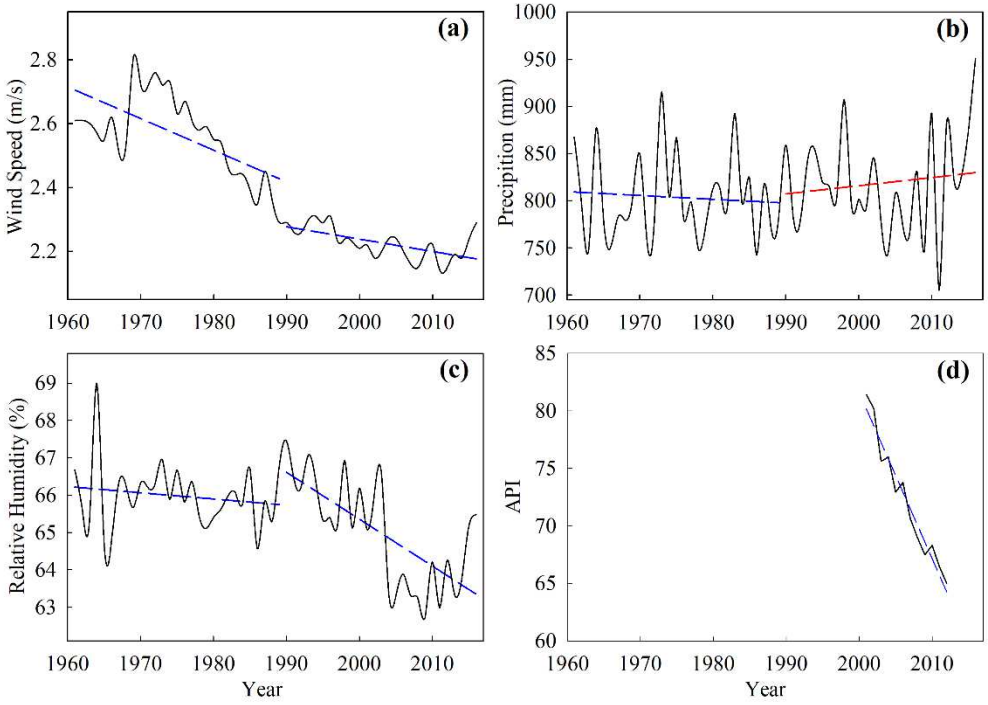

450

451 **Fig. 11** Changes in (a) wind speed; (b) precipitation; (c) relative humidity from 1961 to 2016

452 (divided by 1989); and (d) API during 2001-2012 in mainland China.

453 **Table 5** Regression coefficients of each empirical model in mainland China during 1961-

454 2016.

Model	Model Formula	R^2
Linear	$\frac{S}{S_0} = 0.1790 + 0.5700\frac{H}{H_0}$	0.8190
Quadratic	$\frac{S}{S_0} = 0.1725 - 0.0701\frac{H}{H_0} + 0.6341\left(\frac{H}{H_0}\right)^2$	0.8197
Cubic	$\frac{S}{S_0} = 0.1594 + 0.8472\frac{H}{H_0} - 1.2644\left(\frac{H}{H_0}\right)^2 + 1.0493\left(\frac{H}{H_0}\right)^3$	0.8252
Modified logarithmic	$\frac{S}{S_0} = 0.1603 + 0.8046\log\left(\frac{H}{H_0} + 1\right)$	0.8186
Linear logarithmic	$\frac{S}{S_0} = 0.1698 + 0.3073\frac{H}{H_0} + 0.3073\log\left(\frac{H}{H_0} + 1\right)$	0.8190
Exponential	$\frac{S}{S_0} = 0.3448 - 0.1357\exp\left(\frac{H}{H_0}\right)$	0.8030

References

Ahmad, M.J. and Tiwari, G.N., 2011. Solar radiation models - A review. International Journal of Energy Research, 35: 271-290.

Akinoğlu, B.G. and Ecevit, A., 1990. Construction of a quadratic model using modified Ångstrom coefficients to estimate global solar radiation. Solar Energy, 45(2): 85-92.

Al-Mostafa, Z.A., Maghrabi, A.H. and Al-Shehri, S.M., 2014. Sunshine-based global radiation models: A review and case study. Energy Conversion and Management, 84: 209-216.

Almorox, J. and Hontoria, C., 2004. Global solar radiation estimation using sunshine duration in Spain. Energy Conversion and Management.

Angstrom, A., 1924. Solar and terrestrial radiation. 19. Monthly Weather Review.

Augustine, J.A. and Dutton, E.G., 2013. Variability of the surface radiation budget over the United States from 1996 through 2011 from high‐quality measurements. Journal of Geophysical Research: Atmospheres, 118(1): 43-53.

Bahel, V., H., B. and R., S., 1987. A correlation for estimation of global solar radiation. Energy, 12(2): 131-135.

Bernaola-Galván, P., Grosse, I., Carpena, P., Oliver, J.L., Román-Roldán, R. and Stanley, H.E., 2000. Finding borders between coding and noncoding DNA regions by an entropic segmentation method. Physical Review Letters, 85(6): 1342-1345.

Black, J.N., Bonython, C.W. and Prescott, J.A., 1954. Solar radiation and the duration of sunshine. Quarterly Journal of the Royal Meteorological Society, 80(344): 231-235.

Chan, C.K. and Yao, X.H., 2008. Air pollution in mega cities in China. Atmospheric Environment, 42(1): 1-42.

478 Che, H.Z., Shi, G.Y., Zhang, X.Y., Arimoto, R., Zhao, J.Q., Xu, L., Wang, B. and Chen, Z.H.,
479 2005. Analysis of 40 years of solar radiation data from China, 1961–2000. Geophysical
480 Research Letters, 32(32): 2341-2352.
481 Chen, S.Y., Zhang, K.L., Xing, X.B. and Dong, A.X., 2010. Climatic change of sunshine
482 duration in Northwest China during the last 47 years. Journal of Natural Resources,
483 25(7): 1142-1152.
484 Cooper, P.I., 1969. Absorption of radiation in solar stills. Solar Energy, 12(3): 333-346.
485 Coppolino, S., 1994. A new correlation between clearness index and relative sunshine.
486 Renewable Energy, 4(4): 417-423.
487 Duffie, J.A., Beckman, W.A. and Worek, W.M., 1991. Solar engineering of thermal processes,
488 2nd ed. Wiley.
489 Fan, J.L., Wu, L.F., Zhang, F., Cai, H., Zeng, W., Wang, X. and Zou, H., 2019. Empirical and
490 machine learning models for predicting daily global solar radiation from sunshine
491 duration: A review and case study in China. Renewable and Sustainable Energy Reviews,
492 100: 186-212.
493 Fei, Y. and Xia, X.A., 2015. Interannual and decadal variations of surface solar radiation over
494 East China in the first half of the 20th century. Atmospheric and Oceanic Science Letters,
495 8(05): 314-319.
496 Feng, G.L., Gong, Z.Q., Dong, W.J. and Li, J.P., 2005. Abrupt climate change detection based
497 on heuristic segmentation algorithm. Acta Physica Sinica(11): 5494-5499.
498 Feng, Z.H., Guo, B., Ren, S.J. and Li, Y., 2019. Reduction in sunshine duration and related
499 factors over mainland China during 1961-2016. Energies, 12(24): 4718.
500 Gao, Y., Ma, S., Wang, T., Wang, T., Gong, Y., Peng, F. and Tsunekawa, A., 2020. Assessing

501 the wind energy potential of China in considering its variability/intermittency. Energy
502 Conversion and Management, 226: 113580.
503 Hassan, G.E., Youssef, M.E., Mohamed, Z.E., Ali, M.A. and Hanafy, A.A., 2016. New
504 temperature-based models for predicting global solar radiation. Applied Energy, 179:
505 437-450.
506 Hou, G., Sun, H., Jiang, Z., Pan, Z., Wang, Y., Zhang, X., Zhao, Y. and Yao, Q., 2016. Life
507 cycle assessment of grid-connected photovoltaic power generation from crystalline
508 silicon solar modules in China. Applied Energy, 164(feb.15): 882-890.
509 Hu, Z., Zhen, Yang, S. and Wu, R., 2003. Long‐term climate variations in China and global
510 warming signals. Journal of Geophysical Research: Atmospheres, 108(D19): 4614.
511 Iqbal, M., 1983. An introduction to solar radiation. Space Science Reviews, 39: 387–390.
512 Kaiser, D.P. and Qian, Y., 2002. Decreasing trends in sunshine duration over China for 1954-
513 1998: Indication of increased haze pollution? Geophysical Research Letters, 29(21): 38-
514 31-38-34.
515 Kazaz, A. and Adiguzel Istil, S., 2019. A comparative analysis of sunshine duration effects in
516 terms of renewable energy production rates on the LEED BD+ C projects in Turkey.
517 Energies, 12(6): 1116.
518 Kendall, M.G., 1948. Rank correlation methods. British Journal of Psychology.
519 Lin, C., Yang, K., Huang, J., Tang, W.J., Qin, J., Niu, X., Chen, Y., Chen, D., Lu, N. and Fu,
520 R., 2015. Impacts of wind stilling on solar radiation variability in China. Entific Reports,
521 5: 15135.
522 Liu, J.D., Linderholm, H., Chen, D., Zhou, X., Flerchinger, G.N., Yu, Q., Du, J., Wu, D.,
523 Shen, Y. and Yang, Z., 2015. Changes in the relationship between solar radiation and

524 sunshine duration in large cities of China. Energy, 82: 589-600.
525 Lu, R.Y. and Ye, H., 2011. Decreasing trend in summer precipitation over the Western
526 Sichuan Basin since the 1950s. Atmospheric and Oceanic Science Letters, 04(2): 114-
527 117.
528 Luo, H., Han, Y., Lu, C., Yang, J. and Wu, Y., 2019. Characteristics of surface solar radiation
529 under different air pollution conditions over Nanjing, China: observation and simulation.
530 Advances in Atmospheric Sciences volume, 36(10): 1047-1059.
531 Pazikadin, A.R., Rifai, D., Ali, K., Malik, M.Z. and Faraj, M.A., 2020. Solar irradiance
532 measurement instrumentation and power solar generation forecasting based on Artificial
533 Neural Networks (ANN): A review of five years research trend. Science of The Total
534 Environment, 715: 136848.
535 Pinker, R.T., Zhang, B. and Dutton, E.G., 2005. Do satellites detect trends in surface solar
536 radiation? Science, 308(5723): 850-854.
537 Prescott, J.A., 1940. Evaporation from a water surface in relation to solar radiation.
538 Transactions of the Royal Society of South Australia, 46: 114-118.
539 Rabaia, M.K.H., Abdelkareem, M.A., Sayed, E.T., Elsaid, K., Chae, K.-J., Wilberforce, T.
540 and Olabi, A., 2020. Environmental impacts of solar energy systems: A review. Science
541 of The Total Environment, 754: 141989.
542 Ren, J., Lei, X., Zhang, Y., Wang, M. and Xiang, L., 2017. Sunshine duration variability in
543 Haihe River Basin, China, during 1966–2015. Water, 9(10): 770.
544 Sang, Y.F., Wang, Z.G. and Liu, C.M., 2014. Comparison of the MK test and EMD method
545 for trend identification in hydrological time series. Journal of Hydrology, 510(3): 293-
546 298.

547 Song, Z.Y., Chen, L.T., Wang, Y.J., Liu, X., Lin, L. and Luo, M., 2019. Effects of urbanization
548 on the decrease in sunshine duration over eastern China. Urban Climate, 28: 100471.
549 Stanhill, G., 2005. Global dimming: A new aspect of climate change. Weather, 60(1): 11-14.
550 Súri, M., Huld, T.A. and Dunlop, E.D., 2005. PV-GIS: a web-based solar radiation database
551 for the calculation of PV potential in Europe. International Journal of Solar Energy,
552 24(2): 55-67.
553 Tao, S.L., Qi, Y.M., Shen, S.H., Li, Y.H. and Zhou, Y., 2016. The spatial and temporal
554 variation of solar radiation over China from 1981 to 2014. Journal of Arid Land
555 Resources and Environment, 30(11): 143-147.
556 Wang, Y.W. and Wild, M., 2016. A new look at solar dimming and brightening in China.
557 Geophysical Research Letters, 43(22).
558 Wang, Y.W. and Yang, Y.H., 2014. China's dimming and brightening: evidence, causes and
559 hydrological implications. Annales Geophysicae, 32(1): 41-55.
560 Wang, Y.W., Yang, Y.H., Han, S.M., Wang, Q.X. and Zhang, J.H., 2013. Sunshine dimming
561 and brightening in Chinese cities (1955-2011) was driven by air pollution rather than
562 clouds. Climate research, 56(1): 11-20.
563 Wang, Y.W., Yang, Y.H., Zhou, X.Y., Zhao, N. and Zhang, J.H., 2014. Air pollution is pushing
564 wind speed into a regulator of surface solar irradiance in China. Environmental Research
565 Letters, 10(1): 123-125.
566 Wilberforce, T., Baroutaji, A., El Hassan, Z., Thompson, J., Soudan, B. and Olabi, A.G., 2019.
567 Prospects and challenges of concentrated solar photovoltaics and enhanced geothermal
568 energy technologies. Science of The Total Environment, 659: 851-861.
569 Wild, M., 2005. From dimming to brightening: decadal changes in solar radiation at Earth's

surface. Science, 308(5723): 847-850.

Wild, M., 2009. Global dimming and brightening: A review. Journal of Geophysical Research: Atmospheres, 114(D10).

Wild, M., 2012. Enlightening global dimming and brightening. Bulletin of the American Meteorological Society, 93(1): 27-37.

Wild, M., Trüssel, B., Ohmura, A., Long, C., König‐Langlo, G., Dutton, E.G. and Tsvetkov, A., 2009. Global dimming and brightening: An update beyond 2000. Journal of Geophysical Research: Atmospheres, 114(D10).

Xia, X., 2010. Spatiotemporal changes in sunshine duration and cloud amount as well as their relationship in China during 1954–2005. Journal of Geophysical Research: Atmospheres, 115(D7).

Yang, Y.H., Zhao, N., Hao, X.H. and Li, C.Q., 2009. Decreasing trend of sunshine hours and related driving forces in North China. Theoretical and Applied Climatology, 97(1-2): 91-98.

Yao, W.X., Zhang, C.X., Wang, X., Zhang, Z.G., Li, X. and Di, H., 2018. A new correlation between global solar radiation and the quality of sunshine duration in China. Energy Conversion and Management, 164: 579-587.

Zeng, Y., Cao, Y., Qiao, X., Seyler, B.C. and Tang, Y., 2019. Air pollution reduction in China: Recent success but great challenge for the future. Science of the Total Environment, 663(MAY 1): 329-337.

Zhang, J.Y., Zhao, L., Deng, S., Xu, W. and Zhang, Y., 2017. A critical review of the models used to estimate solar radiation. Renewable and Sustainable Energy Reviews, 70: 314-329.

593 Zheng, Y.F., Yin, Z.Y., Wu, R.J. and Liu, J.J., 2012. Causes and control countermeasures of
594 haze in Beijing-Tianjin-Hebei region. Meteorological and Environmental Research,
595 31(02): 436-445.

596

597 **PS:**

598 **We recommend that color should be used for any figures and tables in print.**

Figures

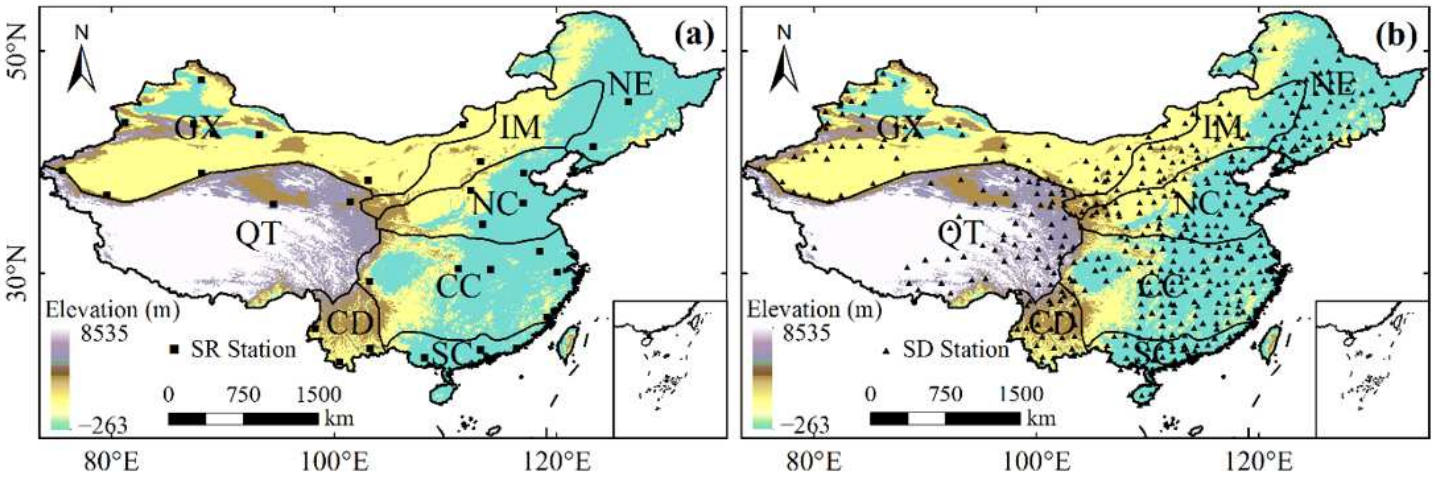

Figure 1

Digital Elevation Model (DEM), eight climate regions and locations of (a) SR; and (b) SD stations in mainland China. Note: The designations employed and the presentation of the material on this map do not imply the expression of any opinion whatsoever on the part of Research Square concerning the legal status of any country, territory, city or area or of its authorities, or concerning the delimitation of its frontiers or boundaries. This map has been provided by the authors.

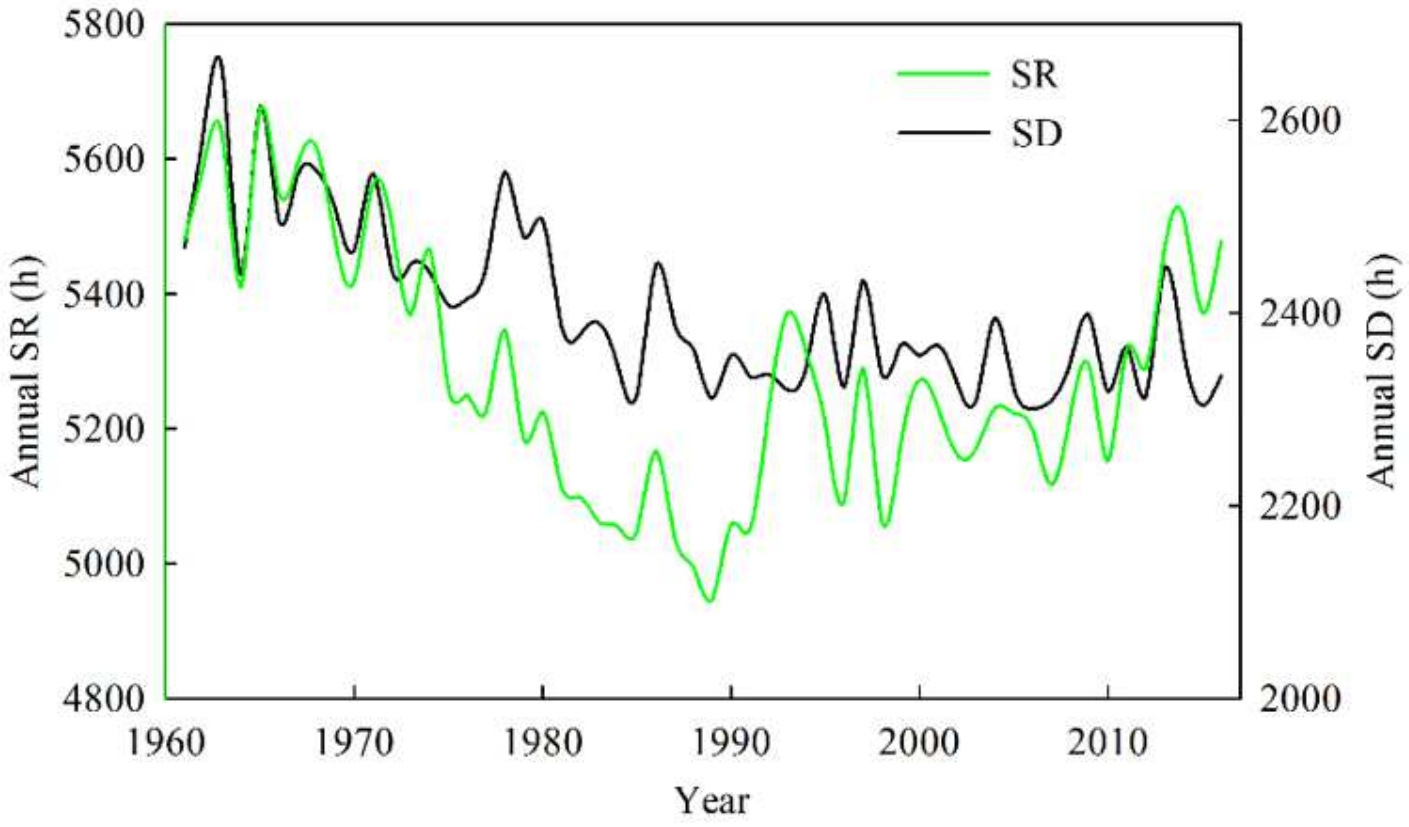

Figure 2

Comparison of the annual mean values of SR and SD in 31 sites during 1961-2016.

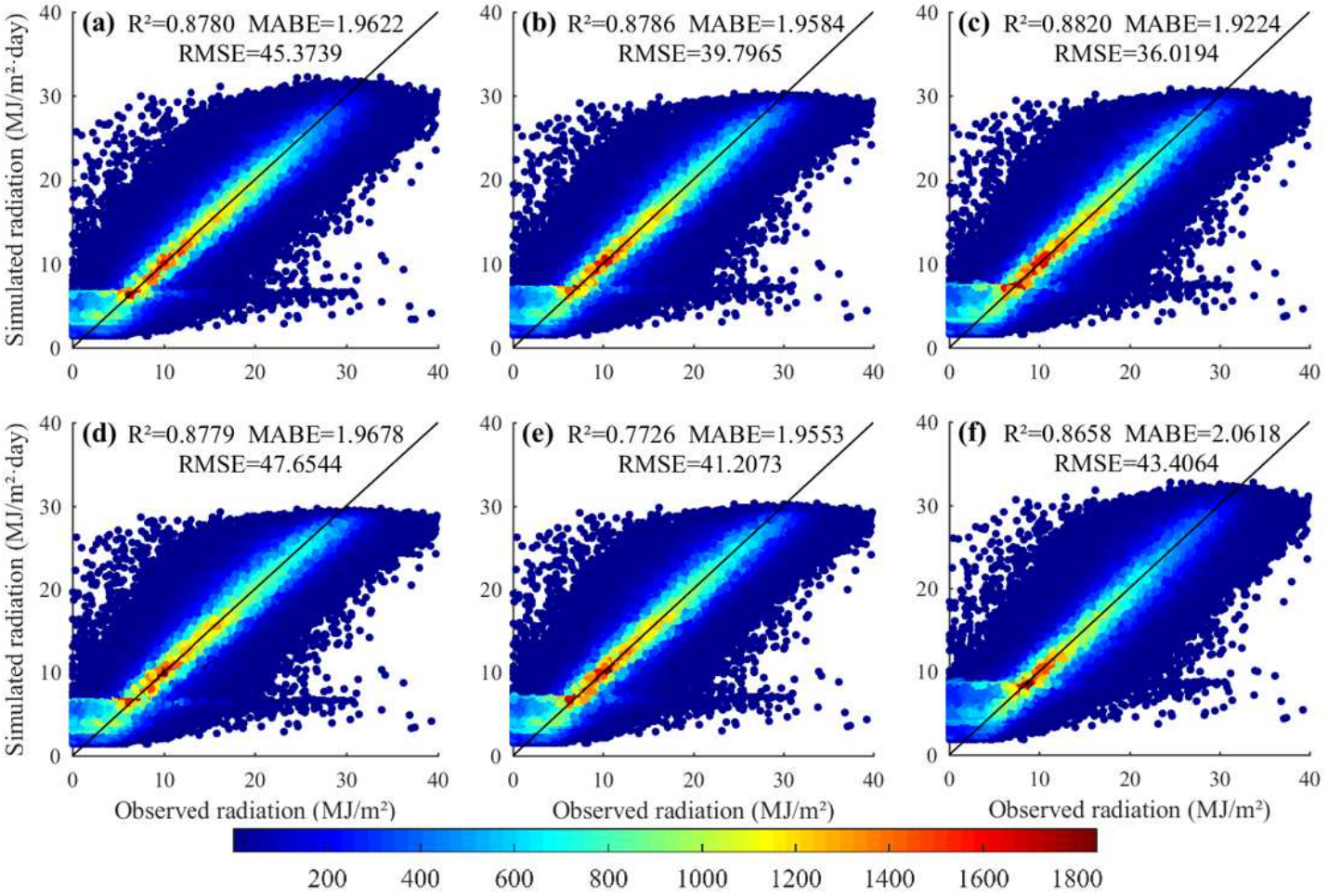

Figure 3

Comparison and error analysis of six models (a) Liner model; (b) Quadratic model; (c) Cubic model; (d) Modified logarithmic model; (e) Linear logarithmic model; and (f) Exponential model (The color of the dots indicates the density of the dots; the red dots are the area with higher density; and black line is y=x).

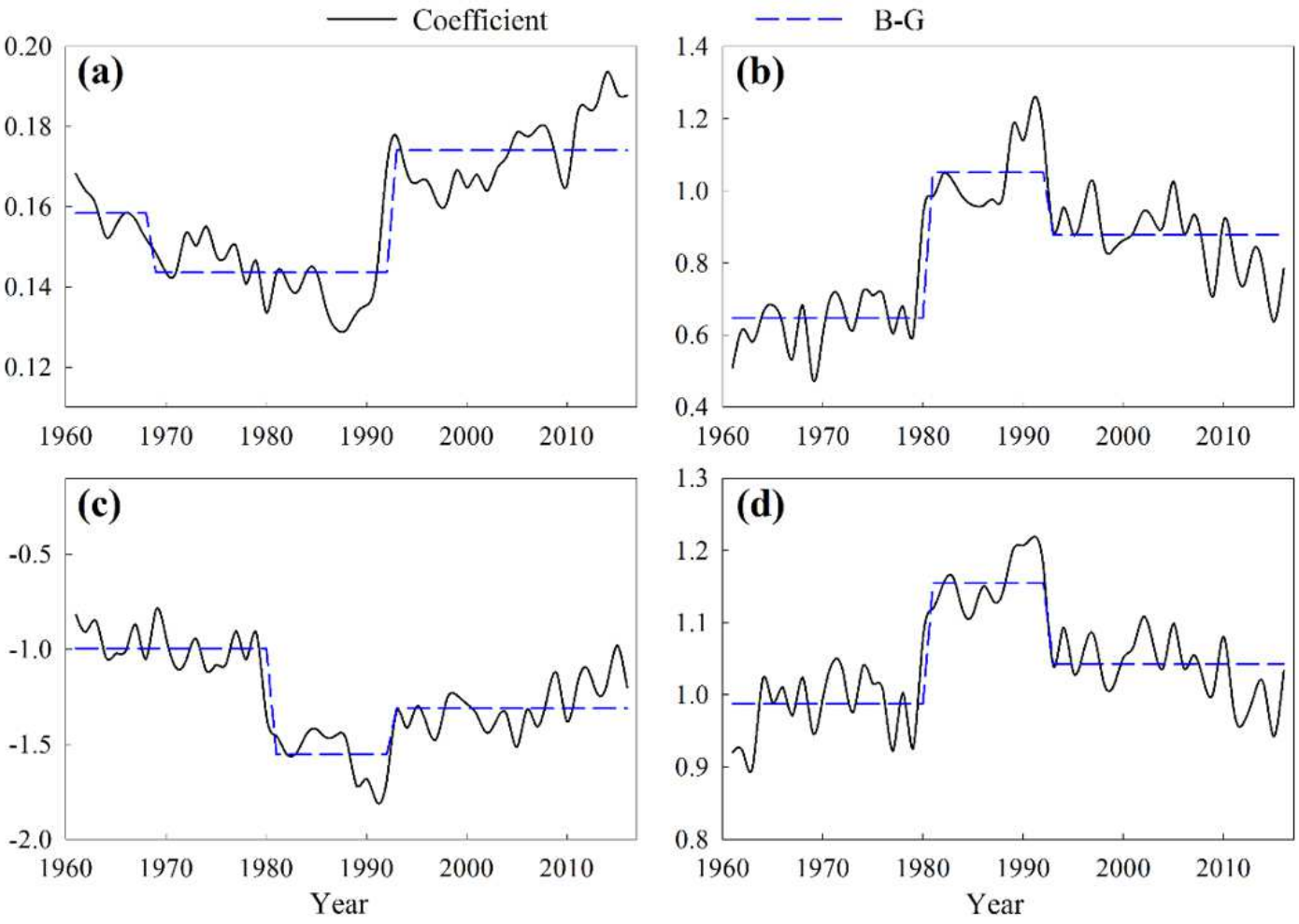

Figure 4

Changes in four coefficients of the Cubic model, 1961-2016. (a), (b), (c) and (d) represent the a, b, c, d coefficients, respectively (Blue line is different mean segmentation obtained by B-G test, and conversion point is mutation time).

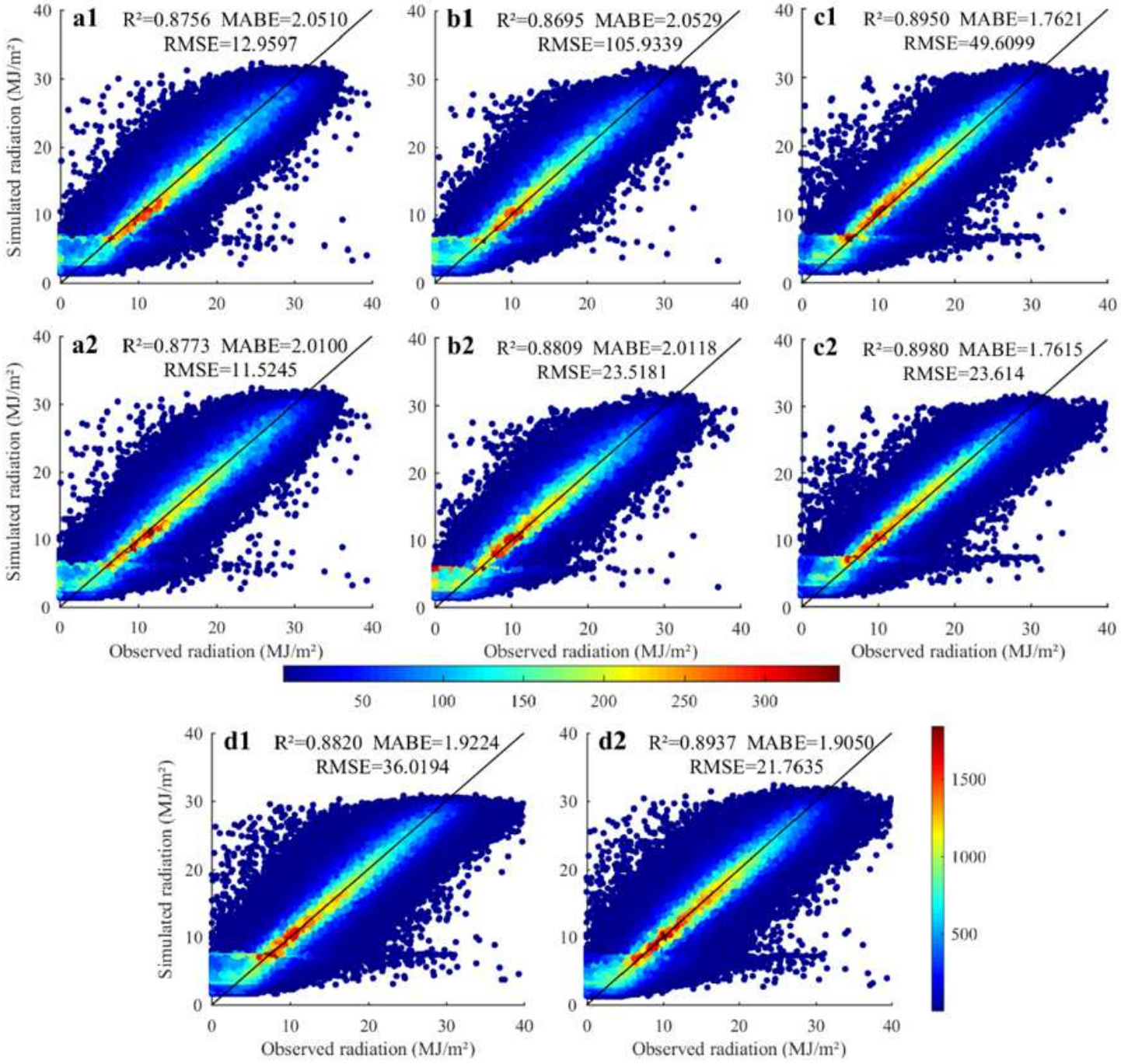

Figure 5

Comparison of simulated and measured values before and after model optimization in different periods (a, b, c and d represent the period of 1961-1979,1980-1991,1992-2016 and 1961-2016 respectively; 1 represents the pre-optimized model and 2 is the post-optimized model. Time period segmentation by primary mutation time of SR. The color of the dots indicates the density of the dots; the red dots are the area with higher density; black line is y=x).

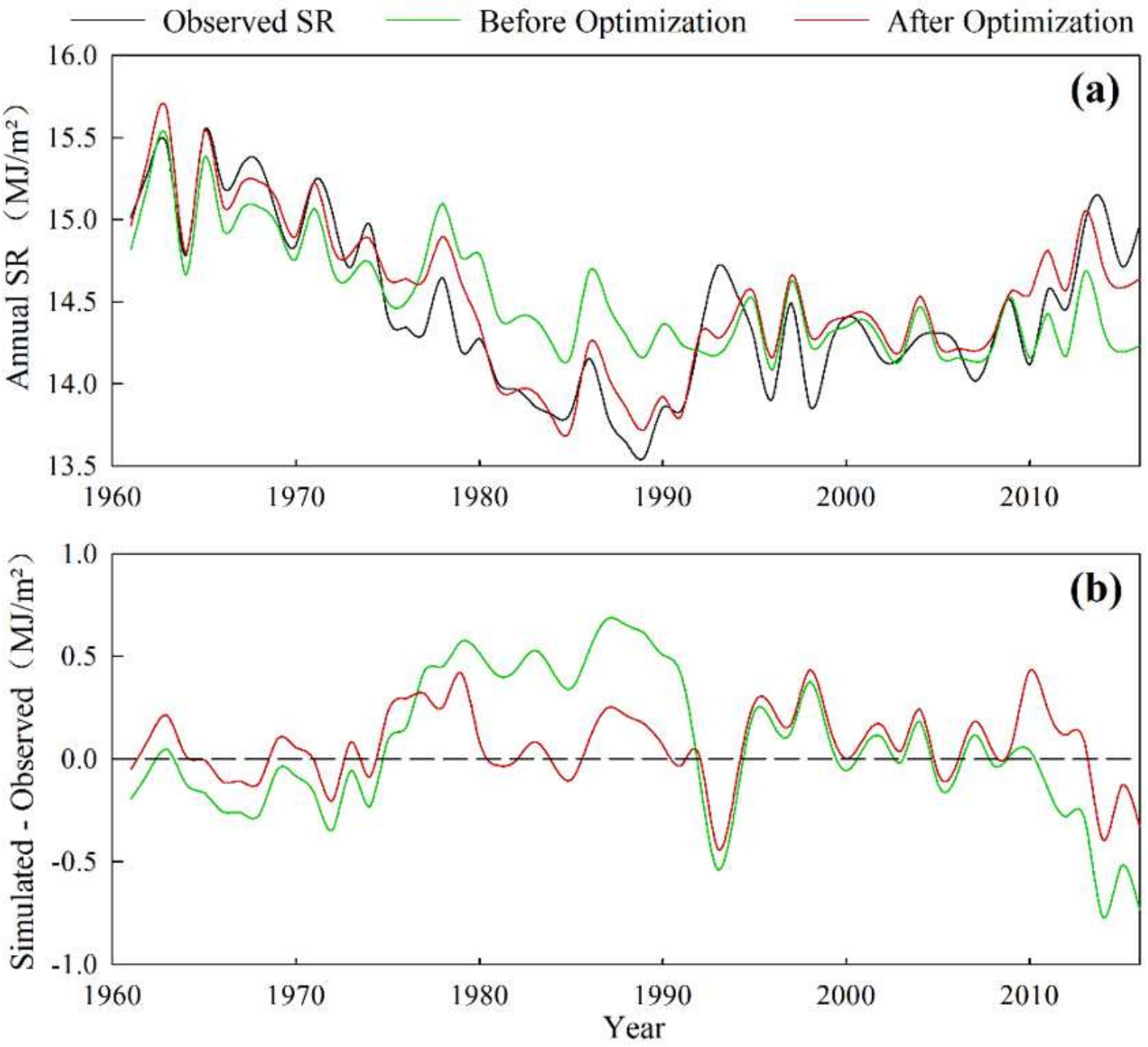

Figure 6

Comparison between simulated and measured values of models before and after optimization: (a) daily radiation exposures; (b) simulated values minus measured values.

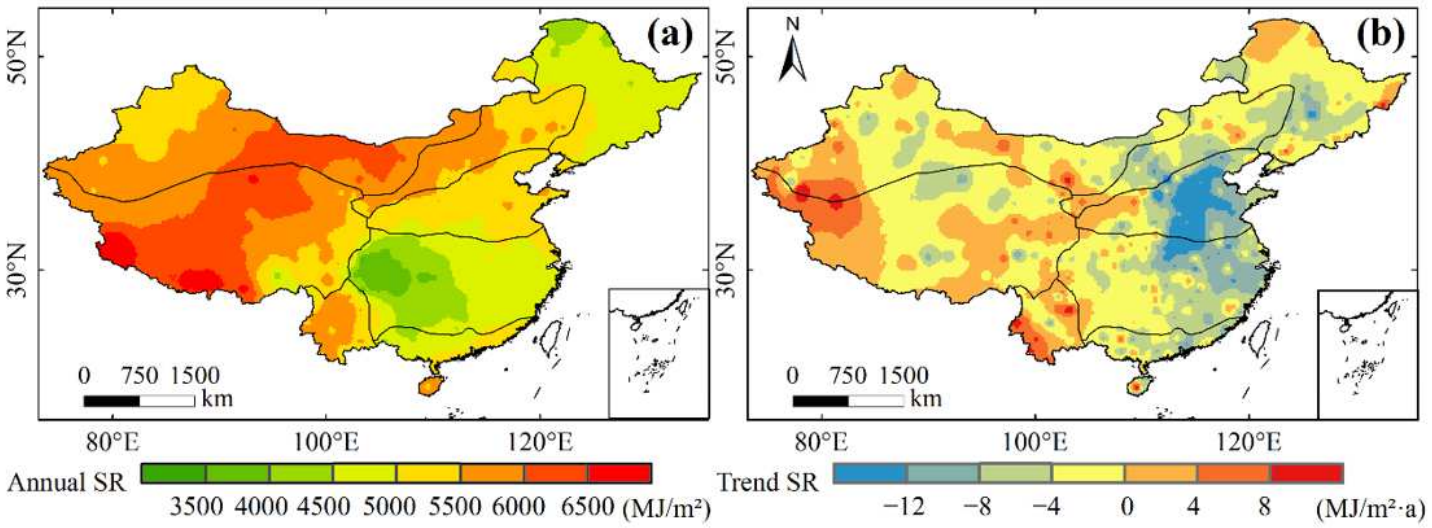

Figure 7

Spatial distribution of (a) annual SR; and (b) tendency rate in mainland China during 1961-2016. Note: The designations employed and the presentation of the material on this map do not imply the expression of any opinion whatsoever on the part of Research Square concerning the legal status of any country, territory, city or area or of its authorities, or concerning the delimitation of its frontiers or boundaries. This map has been provided by the authors.

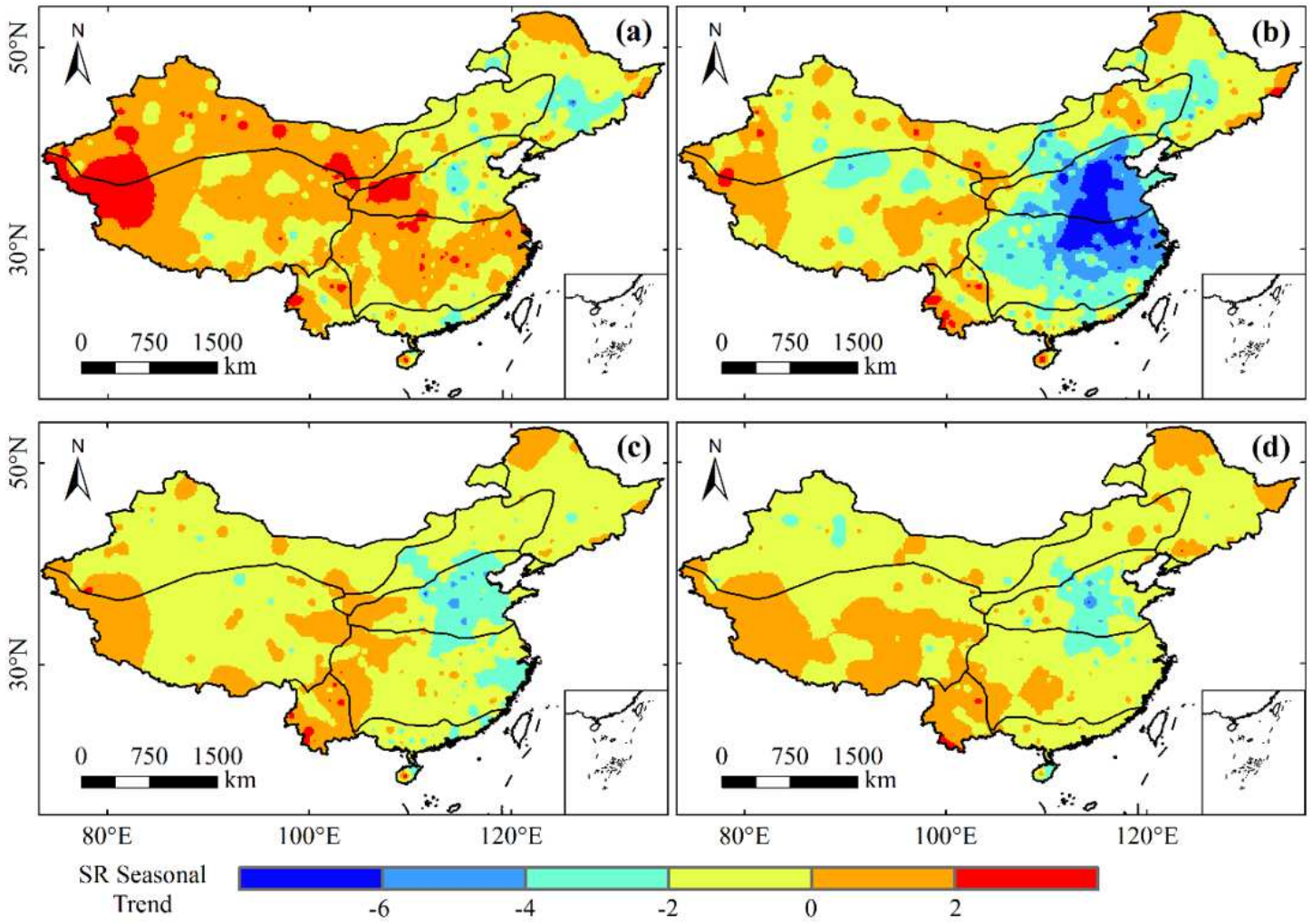

Figure 8

Spatial distribution of seasonal SR in mainland China during 1961-2016 for (a) spring; (b) summer; (c) autumn; and (d) winter. Note: The designations employed and the presentation of the material on this map do not imply the expression of any opinion whatsoever on the part of Research Square concerning the legal status of any country, territory, city or area or of its authorities, or concerning the delimitation of its frontiers or boundaries. This map has been provided by the authors.

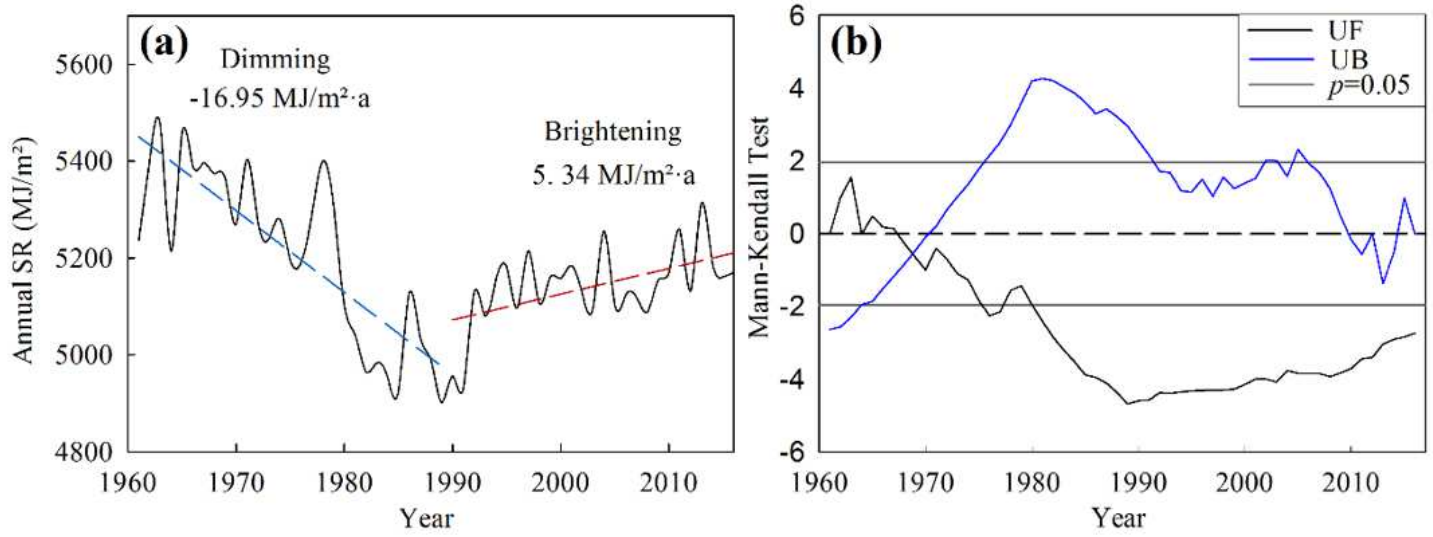

Figure 9

(a) Trends in annual SR; (b) Mann-Kendall test results based on simulated values during 1961-2016 in mainland China.

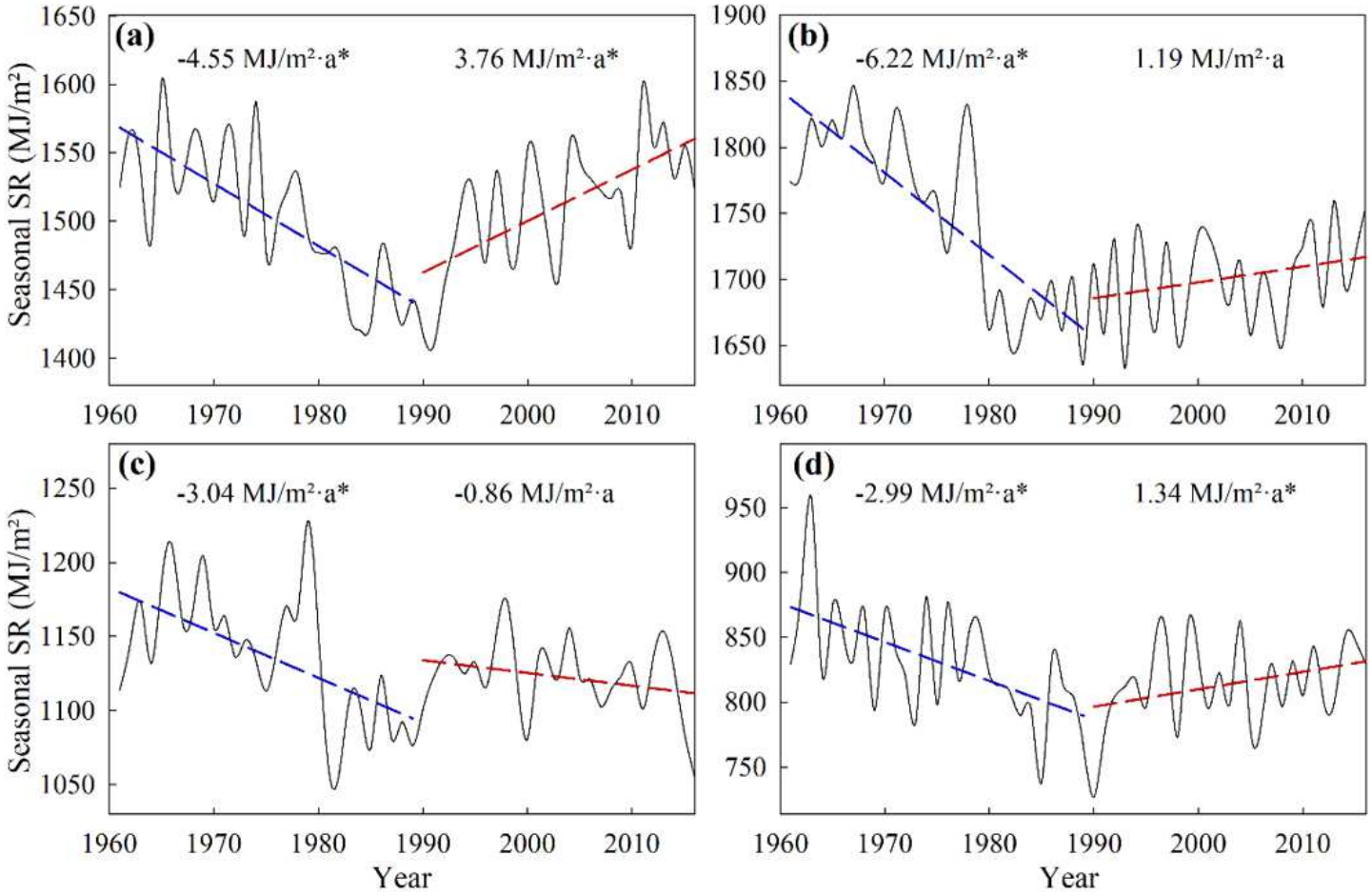

Figure 10

Variations of SR based on simulated values for (a) spring; (b) summer; (c) autumn; and (d) winter in mainland China during 1961-2016 (* refers to passing p<0.05 significance test).

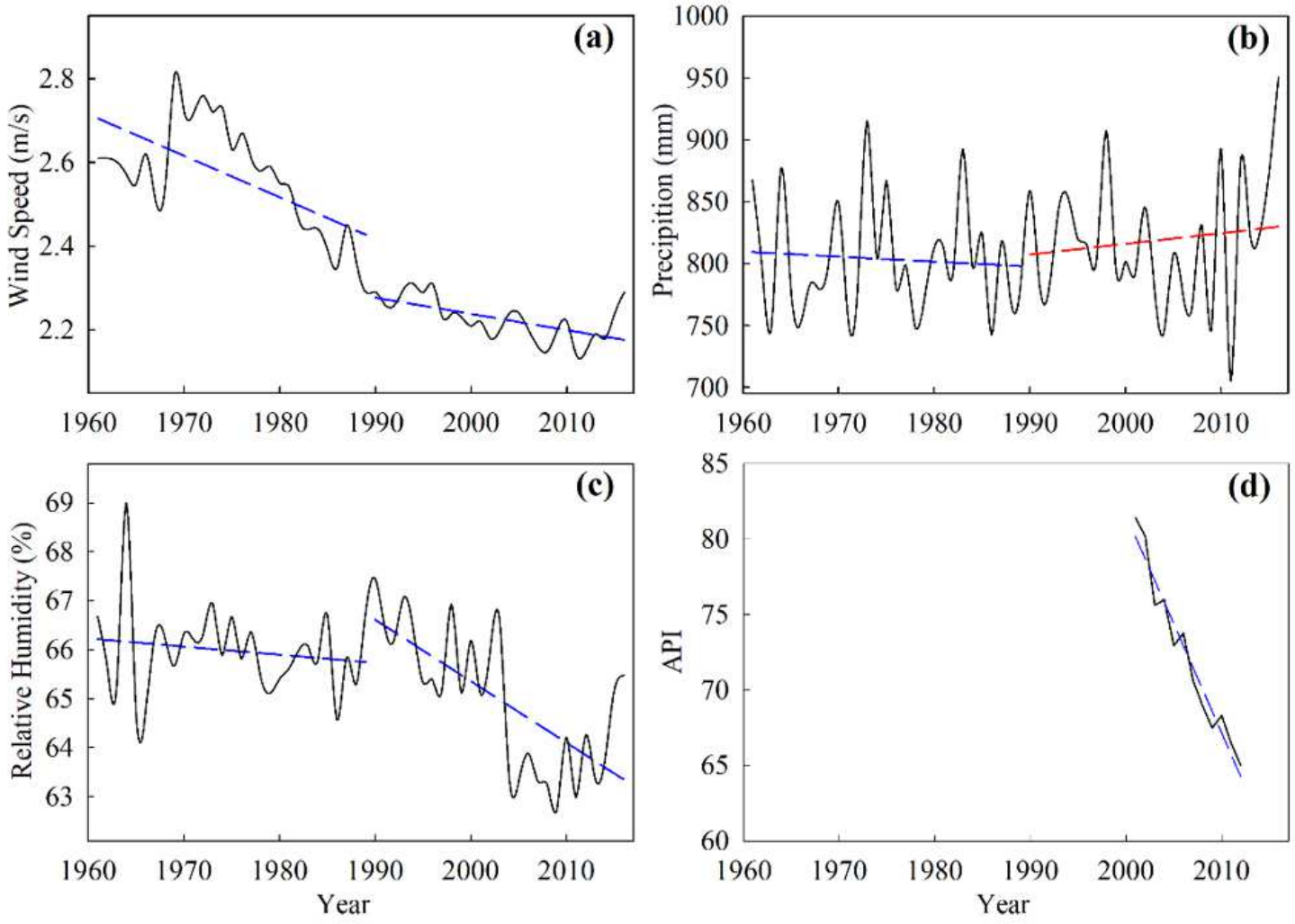

Figure 11

Changes in (a) wind speed; (b) precipitation; (c) relative humidity from 1961 to 2016 (divided by 1989); and (d) API during 2001-2012 in mainland China.

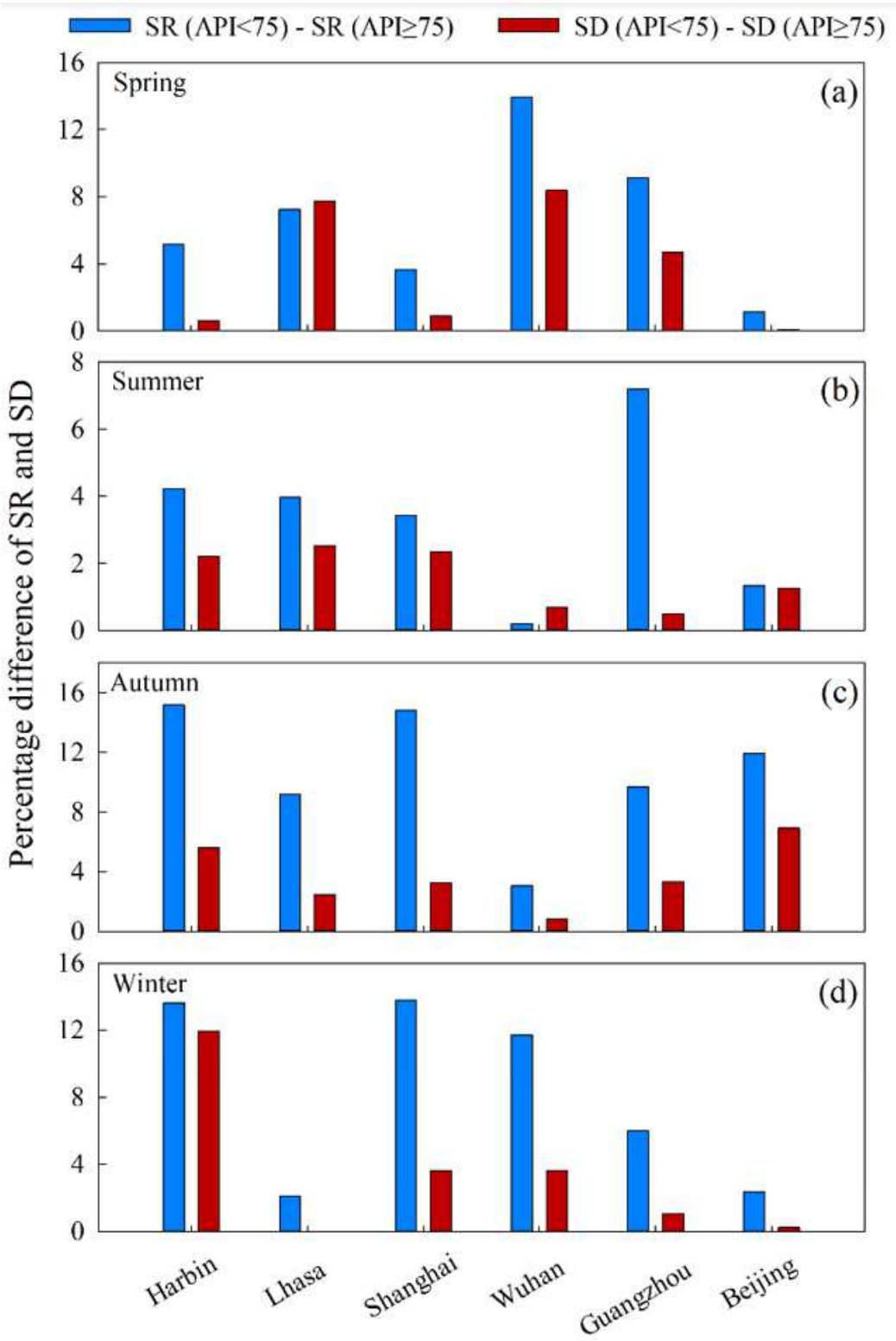

Figure 12

Responses of SR and SD to different pollution levels under clear sky in (a) spring; (b) summer; (c) autumn; and (d) winter (The blue column indicates the percentage difference between SR when API<75 and API≥75, and the red column indicates the percentage difference between SD when API<75 and API≥75).